bioRxiv preprint doi: https://doi.org/10.1101/674150; this version posted June 18, 2019. The copyright holder for this preprint (which was not certified by peer review) is the author/funder, who has granted bioRxiv a license to display the preprint in perpetuity. It is made available under aCC-BY 4.0 International license.

Nature and Nurture integrated through an adjustable Flux Balance Analysis: The impact of cell-nutrition changes on the Warburg effect in hepatocellular carcinoma

Ewelina Węglarz-Tomczak[1*], Thierry D.G.A. Mondeel[1], Diewertje G.E. Piebes[1], Hans V. Westerhoff[1,2,3,4]

[1]Synthetic Systems Biology and Nuclear Organization, Swammerdam Institute for Life Sciences, Faculty of Science, University of Amsterdam, Amsterdam, The Netherlands
[2]Molecular Cell Physiology, Amsterdam Institute for Molecules, Medicines and Systems, Faculty of Science, Vrije Universiteit Amsterdam, Amsterdam, The Netherlands
[3]Manchester Centre for Integrative Systems Biology, School for Chemical Engineering and Analytical Sciences, University of Manchester, Manchester, UK
[4]Systems Biology Amsterdam, Amsterdam, The Netherlands

*Corresponding author
E-mail: ewelina.weglarz.tomczak@gmail.com

bioRxiv preprint doi: https://doi.org/10.1101/674150; this version posted June 18, 2019. The copyright holder for this preprint (which was not certified by peer review) is the author/funder, who has granted bioRxiv a license to display the preprint in perpetuity. It is made available under aCC-BY 4.0 International license.

Abstract

Cancer cells are often home to profound metabolic specialization, such as the Warburg effect wherein cancer cells exhibit high glucose uptake with conversion to lactate in the presence of oxygen. To understand the mechanisms underlying the Warburg effect in hepatocellular carcinoma and to investigate whether and how both the essential nutrient concentrations and the cells' gene expression, impact on this metabolic alteration, we integrated computational genome-wide metabolic modeling with an experimental study on cell lines. We converted transcriptome sequencing (RNA-seq) data from two hepatocellular carcinoma lines HuH7 and PLC/PRF/5 to flux bounds in the most comprehensive human metabolic network model to date, Recon3D. A new method was developed to enable changes in medium concentrations to impact Flux Balance Analyses (FBA) of genome wide metabolic maps. By integrating the two methods, the cells' metabolic behavior could be studied due to applying a new Nature Nurture Scaling (NNS) factor, which assesses the relative importance of gene expression ('Nature') and medium composition ('Nurture'). To examine whether the medium concentrations of glucose and glutamine affect the rate of aerobic glycolysis and growth rate *in vitro*, we further cultured the same two hepatocellular carcinoma lines on media that contained different amounts of glucose and glutamine.

Our integrated approach where expression level (nature) and the environment (nurture) work together, led us to conclude that proliferation, glucose consumption, and lactate production are associated with the presence of glucose, but do not necessarily increase with its concentration when the latter exceeds the physiological concentration. There was no such association with the presence of glutamine. The observed dependencies on glucose concentration could hereby be understood in terms of a balance between Nature and Nurture, as could be the lack of the cells' response to glutamine.

Author summary

Metabolism is directly involved in many human diseases including cancer, and indirectly in virtually all, because disease causes metabolic changes that can accompany or even affect etiologies and be read as biomarkers. The best-known metabolic abnormality in cancer cells is an increased glycolysis followed by lactic acid production even in the presence of oxygen and fully functioning mitochondria, a process known as the Warburg Effect. So-called genome-scale metabolic reconstructions integrate all known metabolic reactions occurring in an organism into a single map. Together with a mathematical method for simulating the optimal balance of metabolic fluxes, this holds promise for studying the mechanisms by which networks control life. We combined this genome-scale metabolic modeling approach

bioRxiv preprint doi: https://doi.org/10.1101/674150; this version posted June 18, 2019. The copyright holder for this preprint (which was not certified by peer review) is the author/funder, who has granted bioRxiv a license to display the preprint in perpetuity. It is made available under aCC-BY 4.0 International license.

with *in vitro* experiments to investigate whether the behavior of cancer cells is determined by their nutrition or/and the expression of their genes. We hereto developed a new method that integrates the genome (*nature*) and the environment (*nurture*) and identified the influence of cell-nutrition changes on the Warburg effect in hepatocellular carcinoma.

Highlights:

1. Cell nutrition and gene expression can now be dealt with simultaneously by FBA through a newly developed Nature Nurture Scaling (NNS) factor.
2. The physiological concentration of glucose is sufficient for the production of lactate by Huh7 and PLC.
3. Huh7 and PLC growth rates are independent of glutamine in media containing glucose.
4. On glutamine alone Huh7 and PLC growth rates are much lower than on glucose alone.

Keywords:

hepatocellular carcinoma, Warburg effect, WarburQ effect, metabolic network modeling, flux balance analysis, genome-scale metabolic map

1. Introduction

Hepatocellular carcinoma (HCC) is among the most common primary liver malignancies [1] and a frequent cause of cancer death [2]. It represents the fifth most common cancer worldwide and over 500 000 new cases are diagnosed per year [3,4]. Hepatotropic viruses such as HBV, HCV, and hepatitis D virus (HDV), and excessive alcohol intake leading to chronic liver disease–and cirrhosis, are the most common cause of HCC worldwide [5,6]. There are other relevant risk factors such as tobacco, obesity, diabetes, metabolic syndrome, and selected aspects of diet [5]. Several factors contribute to the gloom of HCC prognosis: 1) late diagnosis due to lack of symptoms at early stages, 2) recurrence and resistance to chemotherapy, 3) large heterogeneity, and 4) HCCs perfect environment of healthy liver cells providing nutrients to their surroundings. Notwithstanding therapies such as liver resection, transplantation and ablation, the prognosis of HCC is still very poor [7] with five-year survival rates in the 20% range in the United States [8].

Altered metabolism in cancer has been linked to increased tumorigenicity and resistance to chemotherapeutics. The metabolic signatures of cancer cells result from biochemical/metabolic reprogramming (switching) that promote fast growth, survival, proliferation, and long-term maintenance, and are thereby selected for [9]. In most cancer

bioRxiv preprint doi: https://doi.org/10.1101/674150; this version posted June 18, 2019. The copyright holder for this preprint (which was not certified by peer review) is the author/funder, who has granted bioRxiv a license to display the preprint in perpetuity. It is made available under aCC-BY 4.0 International license.

cells the rate of glucose uptake has increased and part of glycolysis-derived pyruvate is diverted to lactate [10-13], which produces much less ATP per glucose than its oxidation to carbon dioxide would. This metabolic signature, known as the Warburg effect [12], enables dividing cells to satisfy anabolic needs for biomass production and is accompanied by a suppression of apoptotic signaling [14,15,16]. The high glucose consumption during the Warburg effect also provides a higher production of reduced nicotinamide adenine dinucleotide phosphate ($NADPH_2$) through the pentose phosphate pathway, which provides electrons to cell proliferation [2,17]. Cancer cells tend to persist in converting much glucose to lactate [10-13], while most normal cells import the glycolysis-derived pyruvate into the mitochondrial matrix. Here the pyruvate is converted to acetyl-coenzyme A, which is oxidized by mainly NAD+ in the Krebs cycle to CO_2 [10,11]. The Warburg effect [12] correlates with tumor aggressiveness and poor patient prognosis in many tumor types, including HCC [14,18-21]. Many cancer cells also have an increased uptake of glutamine [22-26]. The partial catabolism of this glutamine to lactate by cancer cells has been called the WarburQ effect [27]. Some rapidly proliferating cells are particularly dependent on glutamine, and undergo necrosis upon glutamine depletion [25], possibly because glutamine is their main source of nitrogen essential for the synthesis of the amino acids and nucleotides required for cell proliferation.

The excess secretion of lactate would appear to be an inefficient use of cellular resources: each excreted lactate molecule wastes three carbons that might otherwise be utilized for either ATP production [12]. However, the human organism is a perfect host for cancer cells. Lactate produced by cancer cells is picked up from the bloodstream and reconverted to glucose by the liver via the Cori cycle [28], the glucose returning to the blood that then supplies cells, including tumor cells, with this glucose. Similar to lactate, ammonia produced during high glutamine catabolism can also be removed by the liver via the putative glutamine-ammonia cycle [29,30] and returned to the tumor cells as glutamine. According to “Lactate Shuttle” concepts, lactate plays a role in delivery of oxidative and gluconeogenic substrates as well as in cell signaling [31-33]. It includes intracellular (e.g. between the cytosolic and mitochondrial compartments) and extracellular (e.g. between working skeletal muscle and heart) lactate exchanges [31]. The difference between processes e.g. in the healthy heart and skeletal muscles of the host, and cancer cells, is lack of regulation and a-social behavior of cancer cells [27]. The host’s physiology bears the burden of providing a relatively unlimited glucose supply to the cancer cells and a sink for the lactate they secrete [10a,10b]. Thereby the host delivers resources to the proliferating cancer cells at the cost of delivery of these same resources to the other organs, and increasing whole-body Gibbs

bioRxiv preprint doi: https://doi.org/10.1101/674150; this version posted June 18, 2019. The copyright holder for this preprint (which was not certified by peer review) is the author/funder, who has granted bioRxiv a license to display the preprint in perpetuity. It is made available under aCC-BY 4.0 International license.

energy expenditure and multiple organ failure as is highlighted in cancer cachexia. In the case of HCC, resourcing processes are simplified and the liver becomes the host in the host. Refurbished glucose is readily used by local cancer cells and lactate produced by cancer cells is used by liver cells in gluconeogenesis without transportation through the body. The switch is not always quite irreversible: switching of glycolysis to gluconeogenesis in hepatocarcinoma cells lacking gluconeogenesis was possible after application of the corticosteroid medication dexamethasone [34].

A better understanding of the mechanistic links between cell metabolism and survival control may aid in the development of strategies towards a more specific control of HCC progression as well as other types of cancer. The genome-scale metabolic models (GEMs), that are at the core of some bottom-up systems biology approaches, constitute promising tools to study such complex diseases [35,36,37]. Using metabolic reconstructions, researchers can store and continually update information about chemical reactions in a standardized genome wide representation. Various human metabolic maps that represent the entire network of metabolic reactions in a human is known, have been published and their content has been expanded e.g. from 3311 reactions in RECON1 [35a] to 13,543 reactions in RECON3D [37]. Recon3D is not only the most comprehensive human metabolic network model to date, it also includes three-dimensional (3D) metabolite and protein structure data and enables integrated analyses of metabolic functions in humans. GEMs have already been used to predict biomarkers of inborn errors of metabolism [36,38], to identify drug targets [39], to characterize cancer metabolism [40] and to improve the understanding of microbial interactions with the host organism [41,42]. This has been achieved by a computational approach called Flux Balance Analysis (FBA), which enables the computation of optimal steady state flux distributions over genome-scale metabolic maps, optimal in terms of objective functions such as maximum growth yield. Existing computational methodology is able to calculate the implications of quantitative gene expression information for those optimal flux patterns and yields. In reality, the performance of cells may not only be a function of gene expression (which we shall here call ‘Nature’) but also of the metabolic environment of the cells (‘Nurture’), but there is no corresponding FBA methodology yet to take nutrient concentrations into account quantitatively in such calculations.

In the present study, we developed the latter methodology and then use the GEM to predict the influence of the level and ratio of two essential nutrients (glucose and glutamine) in medium on the growth rate and metabolic behavior of cancer cells (HCC), whilst taking into account the transcriptome of those cells. We took advantage of the novel metabolic

bioRxiv preprint doi: https://doi.org/10.1101/674150; this version posted June 18, 2019. The copyright holder for this preprint (which was not certified by peer review) is the author/funder, who has granted bioRxiv a license to display the preprint in perpetuity. It is made available under aCC-BY 4.0 International license.

reconstruction RECON3D [37] and created RECON3D-based metabolic maps that integrate, for the first time, transcriptomic (*nature*) and nutrient concentration (*nurture*) data through a new Flux Balance Analysis approach, by using a new 'Nature Nurture Scaling factor' ('NNS'). Using this integrated approach, *in silico* modeling and *in vitro* experiments on the two hepatocellular carcinoma cell lines HuH7 and PLC/PRF/5, we identify how limitations in expression levels of the metabolic network and nutrient limitations may both cause glucose and glutamine (in)dependencies.

2. Materials and Methods

2.1 Cell lines

For our study we chose two HCC cell lines, i.e. the hepatitis infection–negative Huh7 and the hepatitis infection–positive PLC/PRF/5. Huh7 is a well differentiated hepatocyte-derived cellular carcinoma cell line originating in a liver tumor in a 57-year-old Japanese male. Huh7 is an immortal cell line of epithelial-like, tumorigenic cells. Its cells adhere to the surface of flasks or plates and typically grow as 2D monolayers. Also known as the Alexander hepatoma cell line, PLC/PRF/5 is a human hepatoma originally taken from the liver of a patient with primary liver cell carcinoma who was persistently infected with hepatitis B virus. Also, these cells adhere to the surface of flasks or plates and grow as 2D monolayers [43,44]. Human HCC cells (Huh-7D12 (ECACC 01042712) and PLC/PRF/5 (ECACC 85061113) were purchased from the European Collection of Authenticated Cell Cultures (Salisbury, UK).

2.2. Sources of cell-line specific transcriptomic data

2.2.1 Microarray data

We obtained microarray transcriptomics data from the MERAV database [45] (http://merav.wi.mit.edu/) for both the Huh7 and PLC/PRF/5 cell lines. There was data available from two experiments for Huh7 and one for PLC/PRF/5. All MERAV microarray datasets were renormalized together [45]. For the two Huh7 experimental datasets we averaged the signal per gene between the two experiments.

2.2.2 RNA-seq data

RNA sequencing data for both cell lines was obtained through NCBI's GEO database. Specifically, the RNA-seq dataset from [46] was accessed from: https://www.ncbi.nlm.nih.gov/geo/query/acc.cgi?acc=GSE86602 on November 7th 2018. The RNA-seq dataset pertains to cells grown under conditions somewhat different from the

bioRxiv preprint doi: https://doi.org/10.1101/674150; this version posted June 18, 2019. The copyright holder for this preprint (which was not certified by peer review) is the author/funder, who has granted bioRxiv a license to display the preprint in perpetuity. It is made available under aCC-BY 4.0 International license.

experimental conditions in the present work. The RNA-seq data records transcript levels in terms of a TP(K)M value (Transcripts Per Kilobase Million): i.e. read count normalized by gene length in kilobases (RPK) and divided by 1 million.

2.3 *In silico* analyses

2.3.1 Flux balance analysis

In all simulations in this work we apply the computational technique of Flux Balance Analysis (FBA) [47] to the human genome-wide metabolic map Recon3D [37] using the COBRA toolbox in MATLAB and Python [48,49]. FBA entails the following linear programming problem:

$$Z = c^T v, \text{ such that}$$
$$\boldsymbol{S}v = 0$$
$$\alpha_k \leq v_k \leq \beta_k$$

where *S* is the stoichiometry matrix indicating how many molecules of each metabolite are produced or consumed in each reaction, *v* is the vector of fluxes through all reactions including exchange reactions with the environment of the system considered, *α* and *β* are the vectors of lower and upper bounds on these fluxes, and *c* is a vector of weights generating the linear combination of fluxes that constitutes the objective function *Z*. A flux distribution resulting from FBA therefore satisfies the requirements that each metabolite is produced at the same rate as it is consumed, that the flux boundaries are not exceeded and that the flux distribution maximizes (or minimizes) the objective function Z.

2.3.2 Computational media representation

Ideally, to reproduce experimental cellular conditions accurately in terms of the flux distribution, one should experimentally measure the transport fluxes of all medium components that are taken up or secreted. Using FBA one can then compute the internal flux pattern that should be optimal with respect to a certain objective. However, this is impractical for most mammalian cell line studies as there are quite a few such medium components. Therefore, we here made several assumptions that may be approximately correct under very strict conditions. We assume (i) that the concentrations of the medium components are essentially constant in time, (ii) that the uptake fluxes depend by first-order (i.e. proportional) kinetics on the known substrate concentrations in the medium, thereby producing an uptake rate that can only be reduced by changes in intracellular metabolite concentrations, and (iii) that the proportionality constant is the same for all medium components. Assumption (ii) biochemically implies that in order for the uptake rate to be

bioRxiv preprint doi: https://doi.org/10.1101/674150; this version posted June 18, 2019. The copyright holder for this preprint (which was not certified by peer review) is the author/funder, who has granted bioRxiv a license to display the preprint in perpetuity. It is made available under aCC-BY 4.0 International license.

reduced, something in the downstream network needs to be limiting (i.e. an enzyme concentration). This ultimately has to translate back to increased concentration of metabolites downstream of the uptake step. This is only straightforward if the concentrations are well below the K_m of the transporters, but may be replaced by the options that the uptake reactions run at a V_{max} with respect to their extracellular substrate concentration but that their substrate induces them such that the transporter expression level is proportional (again with the same proportionality constant for all substrates) to (or increasing monotonically with) the extracellular concentration, and that either this induction or the rate is only negatively influenced by intracellular concentrations. Assumption (iii) is unrealistic biochemically, but may be seen as a way to reflect the metabolic potential offered by the media. In accordance with these assumptions, we set the maximal uptake fluxes, for all medium components listed in Table 2, equal to their explicit concentrations in the medium.

In FBA there is a distinction between *exchange* of a metabolite and *transport* of that metabolite. Exchange refers to the net consumption or production of a metabolite and occurs between the extracellular compartment and the outside world. It measures how much substrate that is added to the experimental medium is taken up and used by the cell and how much product leaves the system. In contrast, transport refers only to the transfer of a metabolite between the cytosol and extracellular compartment. Technically, this distinction exists to allow some metabolites to circumvent the steady state requirement in FBA [47]: net catabolism of glucose is consistent with steady state (constant concentrations of metabolites) by allowing exchange with an external compartment to which the steady state requirement is not applied. By implication, if the concentration of a metabolite in the medium supplied to the cells is zero, then the bound (=upper limit) on inward exchange flux is zero. This does not mean that the transport *reaction* of that metabolite is blocked (has bounds of zero) but it does mean that that the transport *flux* will be zero due to lack of substrate. If that extracellular concentration were to go up (by increasing the exchange reaction bound), the metabolite could be imported and transport flux would be possible.

We did not account for metabolic components spilling over from the added serum. We blocked all other uptake of metabolites so that only those compounds listed in Table 2 were allowed to be exchanged in. We did not alter the Recon3D default choices of which metabolites may be net produced by the in-silico cell. This left 1559 metabolites which are allowed to be net-produced by the cell (Supplementary Excel Table 1). Recon3D also contains various so-called *sink* and *demand* reactions which serve as sources and sinks for certain metabolites allowing them to bypass the regular mass-balance. We blocked all such reactions.

bioRxiv preprint doi: https://doi.org/10.1101/674150; this version posted June 18, 2019. The copyright holder for this preprint (which was not certified by peer review) is the author/funder, who has granted bioRxiv a license to display the preprint in perpetuity. It is made available under aCC-BY 4.0 International license.

All uptake reactions and their maximal uptake bounds were taken the same across the six conditions with the exceptions of glutamine and glucose uptake which were varied as specified in Table 1 and 2.

Medium	**Glucose [mM]**	**Glutamine [mM]**
M1	25	4.0
M2	25	0.0
M3	5.6	4.0
M4	5.6	0.0
M5	0.0	4.0
M6	0.0	0.0

Table 1. Media used in experiments in terms of their varying glucose and glutamine concentrations. The media further contained all components like in standard Dulbecco's Modified Eagle Medium (DMEM).

Metabolite	**Uptake bound**	**Metabolite**	**Uptake bound**	**Metabolite**	**Uptake bound**	**Metabolite**	**Uptake bound**
Arginine	0.40	Bicarbonate	44	Nicotinamide	0.033	Thiamin	0.011
Choline	0.028	Histidine	0.2	Valine	0.80	Threonine	0.80
Cysteine	0.20	Isoleucine	0.80	Phenylalanine	0.4	Tryptophan	0.078
Iron (Fe3+)	0.00024	Myo-Inositol	0.04	Phosphate	0.9	Tyrosine	0.40
Folate	0.0091	Potassium	5.3	(R)-Pantothenate	0.0083	Carbon dioxide	1000
Glycine	0.40	Methionine	0.20	Serine	0.40	Oxygen	1000
Water	[54220, 54250, 54100, 54440, 54470, 54500]	Sodium	155	Sulfate	0.81		

bioRxiv preprint doi: https://doi.org/10.1101/674150; this version posted June 18, 2019. The copyright holder for this preprint (which was not certified by peer review) is the author/funder, who has granted bioRxiv a license to display the preprint in perpetuity. It is made available under aCC-BY 4.0 International license.

Glucose	[0,5.6,25]	Leucine	0.80	Pyridoxine	0.019		
Glutamine	[0, 4.0]	Lysine	0.80	Riboflavin	0.0011		

Table 2. Concentrations of metabolites in the DMEM media in mM as listed in the manufacturer's formulation. Our media M1-M6 only differ in the glucose and glutamine concentrations (colored in green) and were exempt of ammonia. All concentrations were effected in-silico as maximal uptake rates which shape and constrain the flux cone of the solutions in FBA (see text). For carbon dioxide and oxygen, a not limiting uptake bound of 1000 was taken. Oxygen was considered non-limiting because the concentration in the medium was in the order of 0.2-0.4 mM (corresponding to air saturated saline) [50] whereas the K_m of cytochrome oxidase for oxygen is some 0.01 mM [51]. Carbon dioxide was considered non-limiting due to its continuous replenishment in the medium.

2.3.3. Adding an acylgroup (*Rtotal*) synthesis reaction to Recon3D [37]

We observed that with the default Recon3D model and given the medium definition discussed above, biomass synthesis was not possible. We traced the problem back to the triglyceride synthesis pathway where in the default Recon3D version a 'source' reaction for triglycerides is present (which allows influx into the cell independent of the presence of triglycerides in the medium; it may be noted that in Recon3D such a source reaction is called a sink reaction, by virtue of sign notation; uptake fluxes are positive, effluxes are positive [47]). Indeed, when temporarily reactivating the triglyceride source reaction (or equivalently activating the triglyceride exchange reaction and adding triglyceride to the medium) a biomass synthesis became possible in all conditions.

Biochemically, triglycerides are synthesized starting from glycerol-3-phosphate and various lipid tails esterified to CoA. Each of these lipid tails can assume any of the three positions in the triglyceride molecule. We observed that without adding triglyceride uptake (or a ditto source) to the metabolic map, the first intermediate in the pathway (lysophosphatidic acid; the monoglyceride with a phosphate on the 3 position) could not be net-produced (see the network diagram in Figure S1 and S2). Inspection of the network revealed that this was due to the need for net input of '*Rtotal'*, 'Rtotal2' and 'Rtotal3' groups in this pathway for which there exists no synthesis reaction in Recon3D. This problem affects biomass flux because multiple metabolites downstream of the triglyceride synthesis pathway (e.g. Phosphatidylcholine, Phosphatidylserine, and Phosphatidylethanolamine, see Table S2), or in branches of it, are explicit components of the biomass used in Recon3D. Recon3D does have the potential to make Stearoyl-CoA, Palmityl-CoA, Oleoyl-CoA and

bioRxiv preprint doi: https://doi.org/10.1101/674150; this version posted June 18, 2019. The copyright holder for this preprint (which was not certified by peer review) is the author/funder, who has granted bioRxiv a license to display the preprint in perpetuity. It is made available under aCC-BY 4.0 International license.

Octadecadienoyl-CoA, but lacks the reactions to associate these with the glycerol moiety: it instead associates Rtotal, Rtotal2 and Rtotal3 to the glycerol moiety, the numbers referring to the position they take in the resulting triglyceride molecule. Recon3D worked around the ensuing problem of lack of biomass synthesis by adding a source for triglycerides. We removed such *dei ex machina* by forbidding source reactions and thereby came across this problem. We solved it by equating *Rtotal*, *Rtotal2* and *Rtotal3* species in Recon3D to a single pool Rtotal and by adding a pooling reaction for lipid tails:

1 Stearoyl-CoA + 1 Palmityl-CoA + 1 Oleoyl-CoA + 1 Octadecadienoyl-CoA <-> 4 Rtotal-CoA

This apparent synthesis reaction merely reflects that the four acyl groups mentioned may be considered a single pool, in the sense that they can largely substitute for each other as lipid tails in biomass. With these two adjustments we have essentially reverted the Recon3D model back to how these reactions were annotated in Recon 2.2 [52] but with a different *Rtotal* synthesis reaction. In Recon2.2 Rtotal synthesis was only possible from Palmityl-CoA and Palmitoleyl-CoA in separate reactions. From Icosanoyl-CoA and Stearoyl-CoA Rtotal2CoA and Rtotal3CoA respectively, could be ~~could~~ synthesized but these metabolites were not connected to anything else in the network. Our grouping of the synthesis of all *Rtotal* into a single reaction, has the advantage that a ratio may be imposed when this is known experimentally. We here took this ratio to be 1:1:1:1 This workaround allowed Recon3D to sustain a positive biomass flux on the medium discussed above. An alternative in which all Rtotal-CoA could be synthesized from any of the four above CoA esters was not here entertained. The resulting 'patched' version of Recon3D is available in the supplementary code and model archive and a list of its reactions and metabolites can be seen in Supplementary Excel Table 2.

All simulations discussed in this section may be reproduced using the scripts in the Supplementary Code Repository.

2.3.4 Mapping transcriptomics data to Reaction Activity Scores with Recon3D [37]

We converted the entrez gene identifiers in Recon3D to their gene symbols (e.g. 8639.1 was converted to AOC3), using the *mygene* module in Python (https://pypi.org/project/mygene/), in order to match them to genes represented in the transcriptomics datasets. Out of the 2248 genes in Recon3D, we were unable to match 103 to the dataset on the basis of their gene symbol alone. We then additionally searched the dataset for known gene aliases and this led us to identifying an additional 87 transcripts. 16

bioRxiv preprint doi: https://doi.org/10.1101/674150; this version posted June 18, 2019. The copyright holder for this preprint (which was not certified by peer review) is the author/funder, who has granted bioRxiv a license to display the preprint in perpetuity. It is made available under aCC-BY 4.0 International license.

genes of Recon3D (see Table S1) we could not identify. These included the three mitochondrial genes encoding the 3 subunits of cytochrome c oxidase. We artificially assigned all these 16 genes a TPM score equal to the maximum TPM score of the genes we could identify for each cell line. Since we do not know whether or not these genes are expressed, we did not want to artificially block them in our model analyses. Setting them to the maximal observed TPM value guarantees that they will not be limiting in any of our analyses.

The existing RNA-sequencing methodology suffers from so-called zero-inflation [53], i.e. the lack of transcripts for genes that are in fact expressed. For data integration this is problematic since a single zero may block an entire pathway. For our dataset we did indeed observe this problem. For example, in the RNA-seq data the serinepalmitoyltransferase-long-chain-base-subunit-3 gene (SPTLC3) which catalyzes the reaction synthesizing 3-dehydrosphinganine (SERPT), has a TPM of zero, and blocking this reaction (after imposing our changes to Recon3D as discussed above) singlehandedly prevents biomass synthesis.

To bypass this problem, we used a microarray dataset and calculated the ratio *R* of the microarray intensity divided by the genome-wide median for each gene that came associated with a TPM score of zero in the RNA-seq dataset. Then we updated such genes' TPM scores and set them equal to the calculated ratio *R* for the microarray dataset multiplied by the genome-wide median in the RNA-seq dataset. Below we will therefore refer to this set of zero-adjusted TPM scores as TPM*. Because the microarray dataset had scores for all genes, this removed all zeros from the dataset. We here neglected any transcriptome difference between the cell lines and experimental conditions used for the microarray and RNA-seq experiments and we assumed that the microarray data were quantitative also at low gene expression.

Recon3D contains an annotated gene-reaction coupling rule for each reaction. Using *AND* and *OR* logic this rule specifies which genes encode proteins that may help catalyze that reaction. The *AND* logic may be used to indicate proteins that consist of more than one subunit, or protein complexes that catalyze reactions whereas the *OR* logic may be used to indicate isoenzymes or alternative configurations of the protein complexes. When integrating the transcriptomics data into the map we turned these Boolean gene-reaction coupling rules into quantitative rules. Here we were inspired by the Metabolic Reaction Enrichment Analysis (MaREA) methodology [54] and the E-flux approach [55]. MaREA had been developed to compare reaction activities between patients rather than between cell lines by assigning a quantitative so-called *Reaction Activity Score* (RAS) to each reaction based on gene expression levels for all proteins that might be involved in the catalysis of that reaction

bioRxiv preprint doi: https://doi.org/10.1101/674150; this version posted June 18, 2019. The copyright holder for this preprint (which was not certified by peer review) is the author/funder, who has granted bioRxiv a license to display the preprint in perpetuity. It is made available under aCC-BY 4.0 International license.

also turning the above Boolean rules into quantitative activities. In order to do this, one needs to know the levels of the corresponding proteins and protein subunits in the cell of interest. We used the mRNA levels as a first approximation to the corresponding protein levels, assuming that the two were proportional. We assigned to each reaction a RAS by summing over isoenzymes (for OR logic) and taking minima of subunits of a complex (for AND logic) the TPM scores for the genes coupled to each reaction. In this way, isoenzymes are thought to contribute additively to the activity of a reaction whereas lack of even one subunit of an enzyme complex can linearly bring down a reaction's activity [54,55].

2.3.5 Constraining fluxes based on RAS scores

To evaluate the implications of the RAS scores for all reactions in the map for the metabolic fluxes through the map we mimicked the approach used in [54,40] and used an approach analogous to the E-Flux approach to map the RAS to flux bounds [55]: we equated RAS scores to those flux bounds, in both directions for reversible reactions (as defined by the map) and in the forward direction for irreversible reactions. Assuming an objective, we then used FBA to compute the implications for the fluxes. More details on this approach are in the Results section.

2.3.6 Data and source code availability

All Python and MATLAB code, Jupyter Notebooks and raw data files are available as part of a Github repository https://github.com/ThierryMondeel/HCC_flux_balance_analysis.

2.4 *In vitro* experiments

2.4.1 Cell culture

The cells were cultured in Dulbecco's modified Eagle's media (DMEM; GibcoBRL, Grand Island, NY, USA) at various initial concentrations of glucose and glutamine (M1-M6, table 1 and 2), supplemented with 10% fetal bovine serum (GibcoBRL, Grand Island, NY, USA), and a solution of 100 U/ml penicillin and 100 µg/ml streptomycin (GibcoBRL, Grand Island, NY, USA), and grown at 37°C in a 5% CO_2 incubator at physiological pH. Cells were seeded on 25 cm^2 cell culture T flasks (Sarstedt, Nümbrecht, Germany) and sub-cultured by trypsin-EDTA (GibcoBRL, Grand Island, NY, USA) treatment. During the experiments reported below the medium was not refreshed.

2.4.2 Growth rate/Cell proliferation assay.

bioRxiv preprint doi: https://doi.org/10.1101/674150; this version posted June 18, 2019. The copyright holder for this preprint (which was not certified by peer review) is the author/funder, who has granted bioRxiv a license to display the preprint in perpetuity. It is made available under aCC-BY 4.0 International license.

Proliferation assays were conducted in 25 cm^2 T flasks, starting with a cell density of $8.2x10^5$ and $5.2x10^5$ cells/ml for Huh7 and PLC, respectively. At the time points indicated, media were collected, cells were washed and trypsinized with a 0.25% (W/V) solution of trypsin (GibcoBRL, Grand Island, NY, USA). The total number of cells in the consequent supernatant was determined by hemocytometer counting (viable plus non-viable). Mean growth rate was determined by counting six non-overlapping sets of sixteen corner squares selected at random, and these four times at each time point.

2.4.2 Metabolic assays

The concentrations of glucose, glutamine and lactate in samples from the cells' supernatant were determined by High Performance Liquid Chromatography (HPLC) based on calibration curves made with standard solutions. The samples were taken from supernatant at the end of experiment, filtered using 0.22μm syringe filters (BGB Analytik Vertrieb GmbH, Rheinfelden, Germany) and stored until measurement in -80℃. HPLC was performed using the HPLC-DAD_RID LC-20AT Prominence (Shimadzu, Columbia, USA) machine with a UV Diode Array Detector SPD-M30A NexeraX2 or/and a Refractive Index Detector RID 20A and an analytical ion-exclusion Rezex ROA-Organic Acid H+(8%) column (250x4.6 mm) with guard column (Phenomenex, Torrance, USA) (5 mM H2SO4 in MilliQ water (18.2 MΩ), isocratic, 0.15 ml/min. flow rate). Injection volume was 15 μl (Autosampler: SIL-20AC, Prominence, Shimadzu), column oven temperature was 55 ºC (Column oven: CTO-20A, Prominence, Shimadzu) and the pressure was 29 bar.

3. Results

3.1 Metabolic genes: expression and activity in two hepatoma cell lines

3.1.1 Differential expression of metabolic genes in Huh7 and PLC

For our two cell lines, the RNA-seq dataset published by Ma et al. [46] reports on 17726 genes. We extracted the RNA-seq records for 2232 out of the 2248 metabolic genes that surface both in this data set and in Recon3D (see Methods). Comparing the mRNA levels (in terms of TPM scores) for the subset of metabolic genes to the genome-wide mRNA levels, we observed that most metabolic genes exhibited a higher than average expression, with a median expression level of ~15 compared to ~1 genome-wide and a mean expression level of ~81 compared to ~39 genome-wide.

We were confronted with a well-known issue with RNA-seq data integration in metabolic models, i.e. zero expression levels, including zeros in mRNAs encoding enzymes

bioRxiv preprint doi: https://doi.org/10.1101/674150; this version posted June 18, 2019. The copyright holder for this preprint (which was not certified by peer review) is the author/funder, who has granted bioRxiv a license to display the preprint in perpetuity. It is made available under aCC-BY 4.0 International license.

catalyzing essential reactions or combinations of enzymes that are essential. Of the 2232 metabolic genes 262 and 310 had TPM scores equal to zero in Huh7 and PLC respectively. Such zeros could be due to true absence or correspond to technical zeros where the gene had in fact been transcribed but was somehow not measured. Technical reasons may include inefficient cDNA synthesis due to tertiary structure formation, amplification bias, or low sequencing depth. Additionally, zeros may occur due to transcription bursting between somehow synchronized individual cells [56] or to small time-windows of expression. Given that an independently obtained set of microarray data might not suffer from quite the same problems, we assigned to genes with zero TPM scores in the RNA seq analysis, alternative TPM scores that reflected the microarray datasets (see Methods).

Huh7 and PLC being both hepatoma cell lines with a different history of oncogenesis, we further expected them to differ mostly in the expression of oncogenes and perhaps other genes involved in signal transduction or management of the genome, but not much in genes encoding metabolic enzymes. With respect to the metabolic genes, we expected both cell lines to be transcriptionally addicted to the same metabolic Warburg rewiring at the level of transcription. With this expectation, a plot of the expression levels Huh7 versus the expression levels of the same genes in PLC should show all genes close to the diagonal line. Although for the majority of genes the correlation fell close to the diagonal, there were quite a few genes for which the expression levels differed between the two cell lines (Figure 1A).

We first looked at the genes that did correlate: In the RNA-seq dataset (prior to correcting for zeros as discussed above), 186 metabolic genes (~8% of the 2232 genes) did not come with any transcript in either cell line. 215 metabolic genes (~10%) exhibited non-zero TPM values below the genome-wide median (~1 TPM), again in both cell lines. Together, these constituted a common set of 401 metabolic genes that were expressed at low level. On the high-abundance side, the two cell lines shared 1422 genes (~63%) that were more highly expressed than the median gene. A 623-genes subset of these 1422 (~28%) was commonly expressed above the genome-wide mean (~39 TPM). These genes behaved in line with our expectation of metabolic similarity between these cell lines. They came however with a possibly important exception of some 425 genes that were off-diagonal in Figure 1A. 415 metabolic genes (~18%) exhibited a TPM score above the genome-wide median in both cell lines and a differential expression ratio of at least 3 (or below ⅓). The data suggests that our expectation was not quite right: there was an appreciable metabolic difference between the two cell lines.

bioRxiv preprint doi: https://doi.org/10.1101/674150; this version posted June 18, 2019. The copyright holder for this preprint (which was not certified by peer review) is the author/funder, who has granted bioRxiv a license to display the preprint in perpetuity. It is made available under aCC-BY 4.0 International license.

In accordance with the above, the expression ratio between the two cell lines was still mostly distributed narrowly around 1. The corresponding probability distribution was largely log-normal, but not quite: it had long 'tails' on either side, suggesting that a disproportionate number of metabolic genes were much more expressed in Huh7 than in PLC and *vice versa* (Figure 1C).

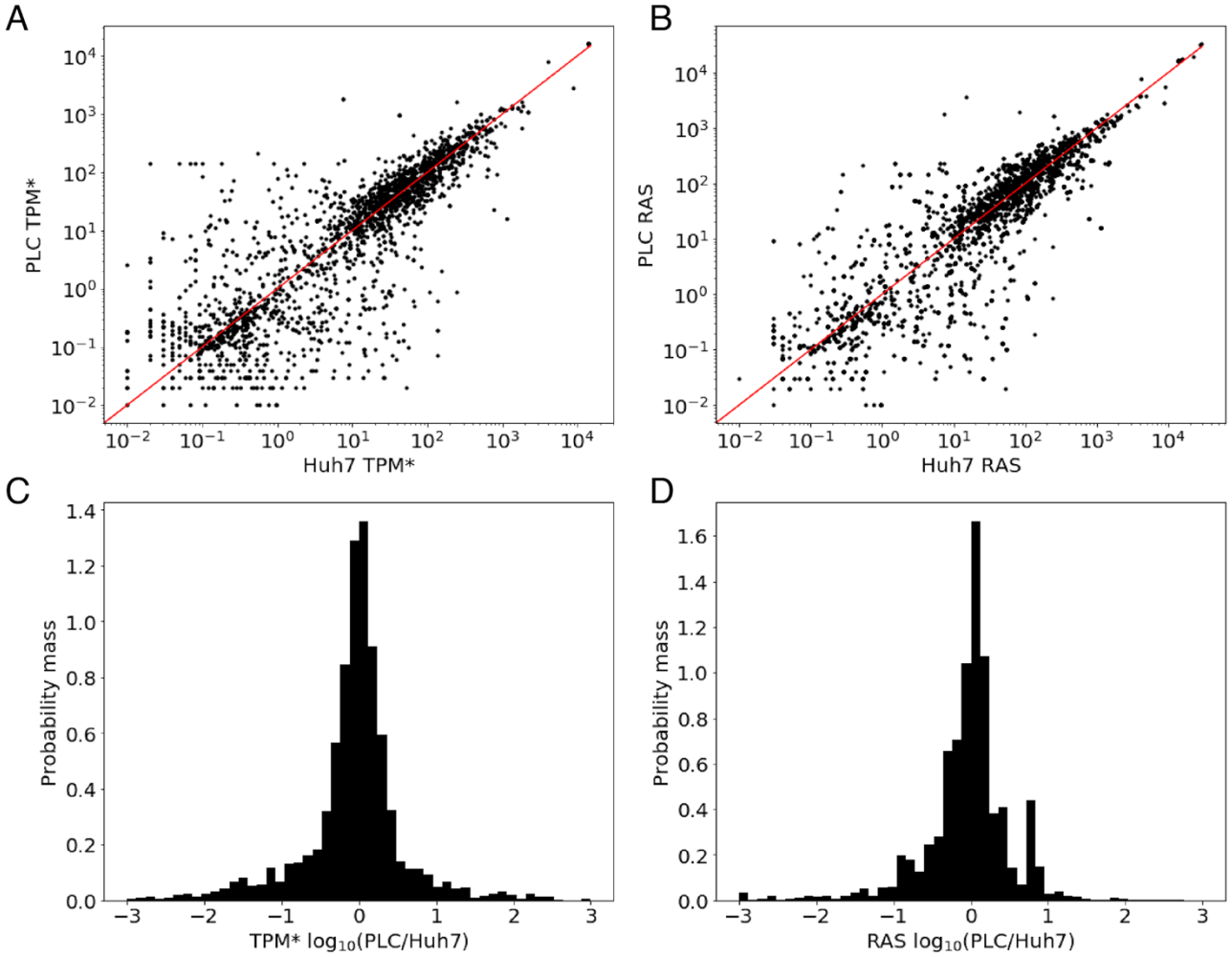

Figure 1. (**A**) Correlation of the mRNA levels (in terms of TPM* scores) between the Huh7 and PLC cell lines for all metabolic genes represented in Recon3D. The line PLC-TPM* = Huh7-TPM* represents theoretical identical scores between the cell lines. (**B**) 2D comparison of the RAS scores (dealing with multi-subunit proteins and isoenzymes) of the Huh7 and PLC cell lines for all metabolic genes represented in Recon3D. (**C**) Histogram of the probability mass function of the $\log_{10}$ of the ratio of the TPM* scores between the two cell lines (PLC relative to Huh7) shown in (**A**). (**D**) Histogram of the probability mass function of the $\log_{10}$ of the ratio of the RAS scores between the two cell lines (PLC relative to Huh7) shown in (**B**).

bioRxiv preprint doi: https://doi.org/10.1101/674150; this version posted June 18, 2019. The copyright holder for this preprint (which was not certified by peer review) is the author/funder, who has granted bioRxiv a license to display the preprint in perpetuity. It is made available under aCC-BY 4.0 International license.

3.1.2 Converting protein subunit levels to Reaction Activity Scores reduces but does not eliminate metabolic differences between Huh7 and PLC

There are at least two reasons why different expression of metabolic genes between two cell lines might not affect the activities of the corresponding biochemical reactions. First, the differences in expression level between the two cell lines could be in enzyme subunits that are abundant as compared to other subunits that are equally expressed. Second, the two cell lines may express different proteins (isoenzymes) that catalyze the same reaction. Recon3D dealt with this issue qualitatively through its gene-reaction coupling rules. We used a quantitative version of these rules to assign a 'Reaction Activity Score' (RAS). The RAS for a metabolic reaction reflects the expression levels of isoenzymes and components of multi-component complexes that may catalyze that reaction (Methods and [40,54-55]). The MaREA data integration framework [54] put forth this approach for integrating transcriptomics data into genome-scale metabolic models based on earlier work on the E-flux approach [55]. Out of the 10601 reactions in Recon3D, 5938 reactions were assigned a RAS in this manner. For the 2999 reactions catalyzed by single genes the RAS scores were taken equal to the TPM values. The remaining 4663 reactions are not linked to any genes: they represent so-called 'exchange reactions' between the cells' immediate environment and the outside world, or non-enzyme-catalyzed reactions and transport within the cells or across their membranes. We left the bounds of such geneless reactions unlimiting at +/- 1000.

We then asked whether the metabolic differences we found between the two cell lines would disappear when correcting for these isoenzyme and enzyme subunit issues by assigning reaction activities. In Figure 1B we correlate the RASs between the two cell lines, and panel 1D shows the distribution over the metabolic genes, of the RAS ratios between the two cell lines. The RAS correlation between the two cell lines is only a little stricter than that of the individual mRNAs. The standard deviation in the RAS ratios is ~14 compared to a standard deviation of ~177 for the TPM* ratios. The fraction of outliers outside the lognormal distribution of the ratio remains substantial however. Supplementary Excel Table 3 lists the 92 outlier reactions with a $\log_{10}$ RAS ratio > 2 or < -2.

3.2. A new Flux Balance Analysis methodology

3.2.1. Translating mRNA levels to flux bounds for flux balance analysis

Functions of living cells are not determined by any individual reaction but rather by fluxes or concentrations set by pathways consisting of multiple reactions at the same time. For calculating such fluxes, FBA requires flux bounds of the reactions. We here translated the

bioRxiv preprint doi: https://doi.org/10.1101/674150; this version posted June 18, 2019. The copyright holder for this preprint (which was not certified by peer review) is the author/funder, who has granted bioRxiv a license to display the preprint in perpetuity. It is made available under aCC-BY 4.0 International license.

RASs into metabolic map flux bounds using a method inspired by the Metabolic Reaction Enrichment Analysis (MaREA) data integration framework [54]. Even though it has been suggested that RAS scores of individual reactions are better for highlighting metabolic differences among groups of (patient) samples than flux distributions predicted based on those RAS scores, here the interest is in flux distribution predictions. The authors of [54] already applied the E-flux methodology to incorporate the RAS scores into flux bounds. We here propose a variant of that approach, where flux bounds are set proportional to RAS scores, i.e. $b_i = \alpha \cdot RAS_i$, where b_i is the flux bound on reaction i, α is a NNS factor independent of the reaction identity, and RAS_i is the RAS based on the expression levels of enzyme(s) catalyzing reaction i. When reaction i is reversible its forward flux is bounded by b_i and its backward flux is bounded by $-b_i$. When reaction i is irreversible the flux bound in the impossible direction remains zero and the flux bound in the possible direction is set to b_i. Essentially this approach assumes that the V_{max} of any enzyme is proportional with the corresponding mRNA transcript level. This approach shares the shortcomings of the E-flux approach in that it may be inaccurate due to non-proportional translation (protein synthesis) [58], absence of corresponding steady state conditions, or due to the differences in catalytic efficiency (k_{cat}) between enzymes. Notwithstanding these shortcomings, the approach may provide some insight into the potential network effects of changes in gene expression levels. Our variant of the E-flux approach allows us to scale the RNA-seq data, in reference to a specific set of medium uptake bounds (see above).

It is a-priori unclear how large the NNS factor α should be. There are two possible sources of limitation for the model: the medium composition (as represented by maximal exchange rates) and the enzyme expression levels (consequent to transcriptomics). We here wish to examine the case where the enzyme expression levels begin to impose limitations on the model output. We thereto start with high α values, where the enzyme expression levels are not limiting, and maximal biomass flux is determined by substrate concentrations in the medium. Then we decrease α and hence all resulting *metabolic* flux bounds uniformly until we see differential effects on the predicted maximal growth rates across media conditions. Where this occurs significantly, we fix α, which thereby becomes a fitted parameter.

3.2.2 Accounting for medium metabolite concentrations in flux balance analysis

To predict the effects of nutritional differences in terms of all components in the medium including the various concentrations of glucose and glutamine, between our six different medium conditions (see Table 2), on the global metabolic behavior of the two cell lines we

bioRxiv preprint doi: https://doi.org/10.1101/674150; this version posted June 18, 2019. The copyright holder for this preprint (which was not certified by peer review) is the author/funder, who has granted bioRxiv a license to display the preprint in perpetuity. It is made available under aCC-BY 4.0 International license.

modified existing genome-scale flux balance analysis: We equated the upper bound of each uptake reaction to the corresponding metabolite concentration in the medium, setting the bound to zero if the metabolite was absent from the medium. In [54,55] the medium was defined as all exchange reactions open with bounds of -1 and +1. Here we took medium concentrations into account quantitatively. Export was left unlimited for all metabolites that were allowed to be exported in the default Recon3D map (see Supplementary Excel File S2 for the list of such metabolites). As a consequence of this approach the units of the uptake fluxes depend on the units used to define the metabolite concentrations in the medium. Below, we shall deal with this problem somewhat by varying the NNS factor.

3.2.3. Ability to predict a dependence of growth rate on medium composition and transcriptome

We analyzed transcriptomics data with the focus on metabolic differences between the cell lines by computing the steady state flux pattern for the maximal biomass synthesis flux for each medium and for each cell line across a range of values for the NNS factor $\alpha \in [0.01, 1]$ (Figure 2). For either cell line Figure 2 shows that for a NNS factor in excess of 0.3, the predicted growth rates differed between media conditions, the ones at 25 mM glucose being about double those at 5.6 mM glucose. Also, a dependence on glutamine concentrations was predicted, but this dependence was smaller.

When decreasing the NNS factor to below 0.1, this medium dependence disappeared for four out of six modeled medium conditions: the same biomass flux was then predicted which was still significantly higher than that for the remaining two medium conditions at zero glucose (5 and 6). Huh7 predictions for media 1-4 converged already at higher values for α than did the predictions for PLC. Huh7 was predicted to have equal or lower growth rates than PLC across all conditions. Medium 1, followed by medium 2, were predicted to yield the highest biomass fluxes for the high values of α, corresponding (see above) to absence of gene-expression limitations. This reflects the model's sensitivity to carbon input for high α values, since medium 1 and 2 contained the highest levels of glucose. At α= 0.1, the simulations for media 1-4 yielded equal biomass fluxes which were still larger than the predicted fluxes for medium 5 and 6 which lack glucose. This indicates that by reducing the NNS factor, the model can be made more (high α, hence no limitation by low transcription of metabolic genes and thereby limitation by uptake) or less (low α, hence strong limitation by low transcription of metabolic genes) sensitive to variation in concentration of the growth substrate.

bioRxiv preprint doi: https://doi.org/10.1101/674150; this version posted June 18, 2019. The copyright holder for this preprint (which was not certified by peer review) is the author/funder, who has granted bioRxiv a license to display the preprint in perpetuity. It is made available under aCC-BY 4.0 International license.

The fact that media 1-4 converge to similar biomass synthesis flux optima for low levels of α may reflect a shared limiting reaction downstream of (and at a flux bound smaller to the bound of) the exchange reaction the flux bound of which keeps monotonically decreasing with decreasing α. In Figure 3 we summarize the predicted maximal biomass fluxes for the NNS factor α = 0.1, which is at the transition between limitation by extracellular substrate levels and intracellular expression levels. It shows that reduction of glucose concentration does not decrease maximal biomass flux as we observed in *in vitro* experiments (compare Figure 3 and 6A) .

We observe that nontrivial predictions for limitations imposed by medium composition and gene expression can be computed by our new method, such as that (i) both in the absence and in the presence of glutamine the growth rate should be independent of glucose concentrations between 5.6 and 25 mM, yet decrease appreciably in the absence of glucose, (ii) the specific growth rate of Huh7 cells is lower than that of PLC cells, (iii) in the absence of glucose, the cells should be able to grow on glutamine, but (iv) growth rate on glutamine alone should be much lower than on glucose alone.

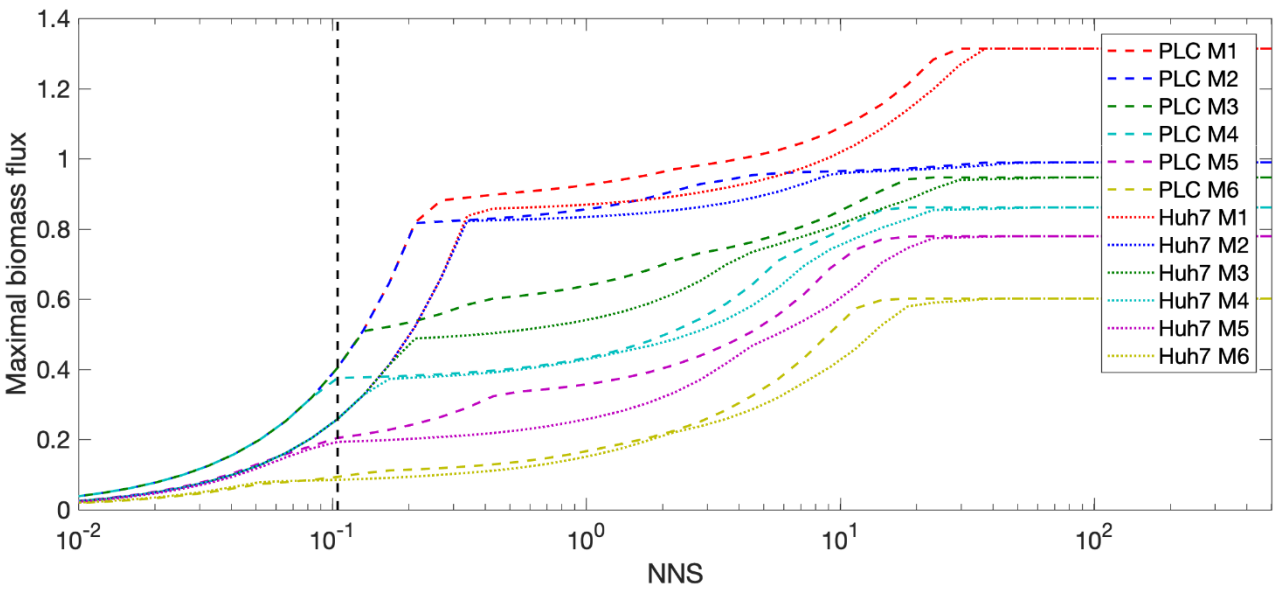

Figure 2. Maximal in-silico biomass flux predictions for Huh7 (dashed lines) and PLC (dotted lines) on six medium conditions versus the NNS factor α used to convert mRNA levels (RNA-seq TPM scores) to flux bounds. The labels M1-M6 refer to the different medium conditions listed in Table 1 and 2 and were effected as proportional uptake (exchange) bounds: Glucose and glutamine were (in mM) 25, 4 (M1), 25, 0 (M2), 5.6, 4 (M3), 5.6, 0 (M4), 0, 4 (M5) and 0, 0 (M6). The dashed black line indicates α= 0.1, the value of the NNS factor that we shall consider more in detail below and at which the maximal biomass flux predictions for M1-M4 become virtually equal for both cell lines.

bioRxiv preprint doi: https://doi.org/10.1101/674150; this version posted June 18, 2019. The copyright holder for this preprint (which was not certified by peer review) is the author/funder, who has granted bioRxiv a license to display the preprint in perpetuity. It is made available under aCC-BY 4.0 International license.

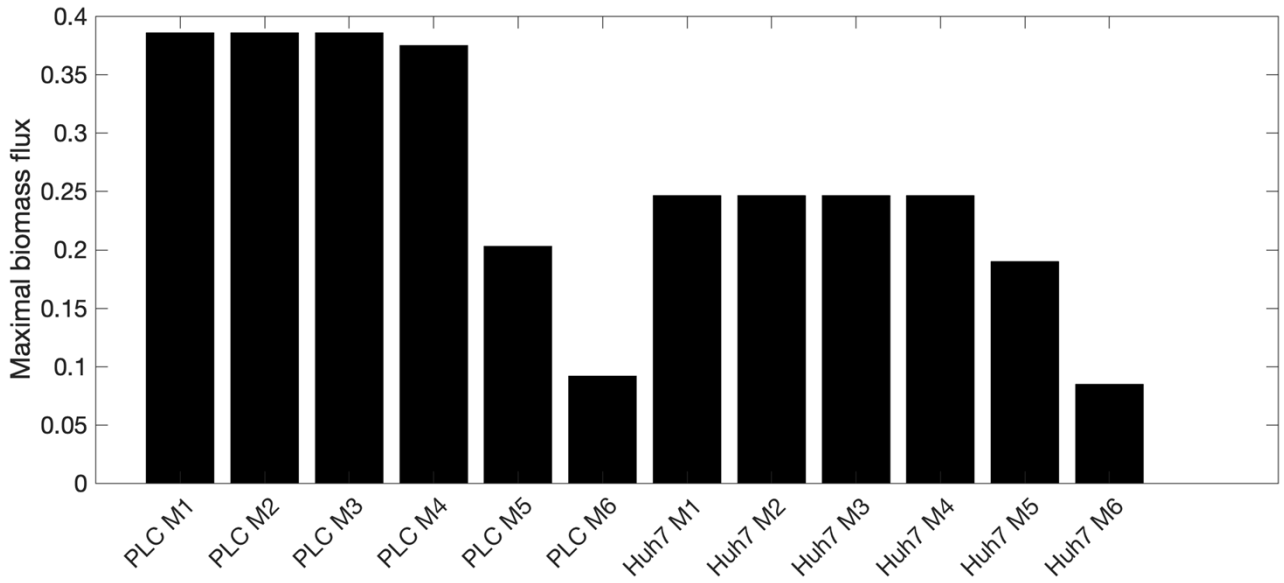

Figure 3. Maximal in-silico biomass flux predictions for PLC and Huh7 across the six different media conditions for a RAS NNS factor of α= 0.1 (as in Figure 2).

3.2.4. Metabolic flux potential as predicted by Flux Variability Analysis

Fluxes through intracellular biochemical reactions are not only determined by the concentrations of the enzymes catalyzing them, but also by metabolic regulation [57], i.e. by the concentrations of intracellular metabolites. FBA is oblivious of metabolic regulation other than that it philosophizes about what flux should be optimal for the cell in view of some objective. The transcriptome and extracellular-concentrations informed flux bounds that we here implemented, merely define ranges of the fluxes rather than that they precisely predict the fluxes. For the precise predictions of fluxes one needs fully dynamic models [58], but the kinetic information required for this approach is missing for mammalian cells. We hereby can only predict the ranges of fluxes that are consistent with transcriptome and extracellular metabolite concentrations and this is done by flux variability analysis.

For the NNS factor value α= 0.1, indicated by the black vertical line in Figure 2, we analyzed each of the 12 models in terms of the possible ranges its production fluxes of lactate, pyruvate, ATP and CO_2 and its uptake fluxes of glucose, glutamine, oxygen and phenylalanine. Here we maintained the maximal biomass flux for each specific medium and transcriptome (i.e. the biomass fluxes listed in Figure 3, which differ between the 12 models) (Figure 4). The results for lactate and pyruvate production are non-negative since these compounds are not in the growth medium and thus cannot be taken up. In order to avoid thermodynamically infeasible ATP synthesis the ATP hydrolysis reaction was non-negative

bioRxiv preprint doi: https://doi.org/10.1101/674150; this version posted June 18, 2019. The copyright holder for this preprint (which was not certified by peer review) is the author/funder, who has granted bioRxiv a license to display the preprint in perpetuity. It is made available under aCC-BY 4.0 International license.

by design. The fluxes in Figure 4 for glutamine and CO_2 can be both negative and positive due to these compounds being present in the medium. If the lower end of its bar in Figure 4 is positive that compound must be produced for the cell to grow at maximal growth rate: it is a primary metabolite. When the upper end of the bar is negative it indicates that the compound needs to be taken up for maximal growth.

In Figure 4 we see that in the media where glucose is present (M1-M4) some glucose uptake is essential for attaining the maximal growth rate. In M5-M6 glucose uptake is always zero due to its absence from the medium. Phenylalanine, an essential amino acid, functions as a positive control. Its uptake proves indeed essential in all media for both cell lines as expected. In most media its uptake rate can vary from the amount of phenylalanine in biomass to 0.4, the rate at which it can be used to provide nitrogen to other parts of anabolism. This maximum uptake rate of 0.4 is the same for all media and both cell lines, reflecting that this corresponds to its concentration in the media. In the absence of glutamine and in the presence of low glucose (M4), PLC needs to make full use of this phenylalanine in order to achieve its maximum growth rate, but Huh7 cells could still vary the amount of phenylalanine used whilst attaining the same growth rate. Maximum lactate, pyruvate and ATP production capabilities track the total amount of carbon in the medium within each cell line, with subtle differences between the two cell lines. The gene expression levels appear to be consistent with shifting to virtually complete metabolism of glucose and glutamine to lactate whilst maintaining the maximum growth rate. At the same biomass production flux, lactate efflux could also be as high as 55 mM, corresponding to 2 lactate per maximum glucose consumed plus one lactate per maximal glutamine consumed. However, in all models, the lactate secretion can also be zero while maintaining maximal growth. This shows that glucose conversion to lactate can vary greatly, and may also reflect that in our models the cells can produce and secrete other compounds such as pyruvate. The *in silico* cells are not addicted to the Warburg effect.

Glutamine uptake is only essential for both PLC and Huh7 in medium 5 and for PLC only in medium 3. In medium 3 for PLC it is then required at a very low amount to achieve optimal growth (as indicated by the upper end of the bar) whereas in medium 5 in both cell lines the maximal uptake bound has to be hit to achieve maximal growth (see the markers at -4). Because (*in silico*) the maximum growth rate of Huh7 is lower it has the luxury of producing glutamine from glucose whilst growing maximally in M3 whereas this is not possible for PLC. Both cell lines may produce glutamine in M1 and M2 owing to the excess glucose in those media. We conclude that the model cells are insensitive to glutamine

bioRxiv preprint doi: https://doi.org/10.1101/674150; this version posted June 18, 2019. The copyright holder for this preprint (which was not certified by peer review) is the author/funder, who has granted bioRxiv a license to display the preprint in perpetuity. It is made available under aCC-BY 4.0 International license.

concentrations in the medium in the presence of high glucose but glutamine-sensitive in the absence of glucose.

In all models a small amount of oxygen must be taken up. CO_2 (either as CO_2 or as bicarbonate) may either be produced or taken up in M1-M3 for both cell lines and M4 for Huh7 and may only be produced in M4 for PLC and M5-M6 for both cell lines. CO_2 uptake might have to do with the reversal of the isocitrate dehydrogenase reaction, which produces isocitrate as substrate for ATP citrate lyase producing cytosolic acetyl CoA for lipid and cholesterol synthesis [27]. For conditions where CO_2 or bicarbonate production is required this may point to oxidative phosphorylation being required for maximal biomass production. Oxygen uptake was essential even in conditions where oxidative phosphorylation (interpreted as CO_2 production) seems not to be required. In these cases, oxygen uptake may be necessary for the synthesis of tyrosine, ~~or of~~ cholesterol and other lipids that are part of the biomass definition and absent from our growth media. We checked that removing cholesterol from the biomass equation reduced the need for oxygen, but it did not remove it.

The possibility to grow at maximum rate in the absence of CO_2 production in some conditions, highlights the possibility for cells to obtain all the Gibbs energy they need for maximal growth only from the conversion of glucose to lactate. This may underlie the selection of the Warburg effect by a-social cells [27]. It does not quite correspond to the Warburg and WarburQ effects however: the *in silico* cells are not addicted to the absence of respiration, as they can still respire all this substrate whilst growing at the same rate. In PLC cells, but not in Huh7 cells, the maximal growth rate in low glucose medium without glutamine (M4) does require oxidative phosphorylation, consistent with the glutamine to lactate pathway elucidated by Damiani et al [27]. These and other apparently minor differences between cell lines in our FVA results are of interest, as they suggest that drugs, in this case ones that inhibit respiration, should be effective against some cancer cells and not others, also depending on extracellular metabolic conditions.

bioRxiv preprint doi: https://doi.org/10.1101/674150; this version posted June 18, 2019. The copyright holder for this preprint (which was not certified by peer review) is the author/funder, who has granted bioRxiv a license to display the preprint in perpetuity. It is made available under aCC-BY 4.0 International license.

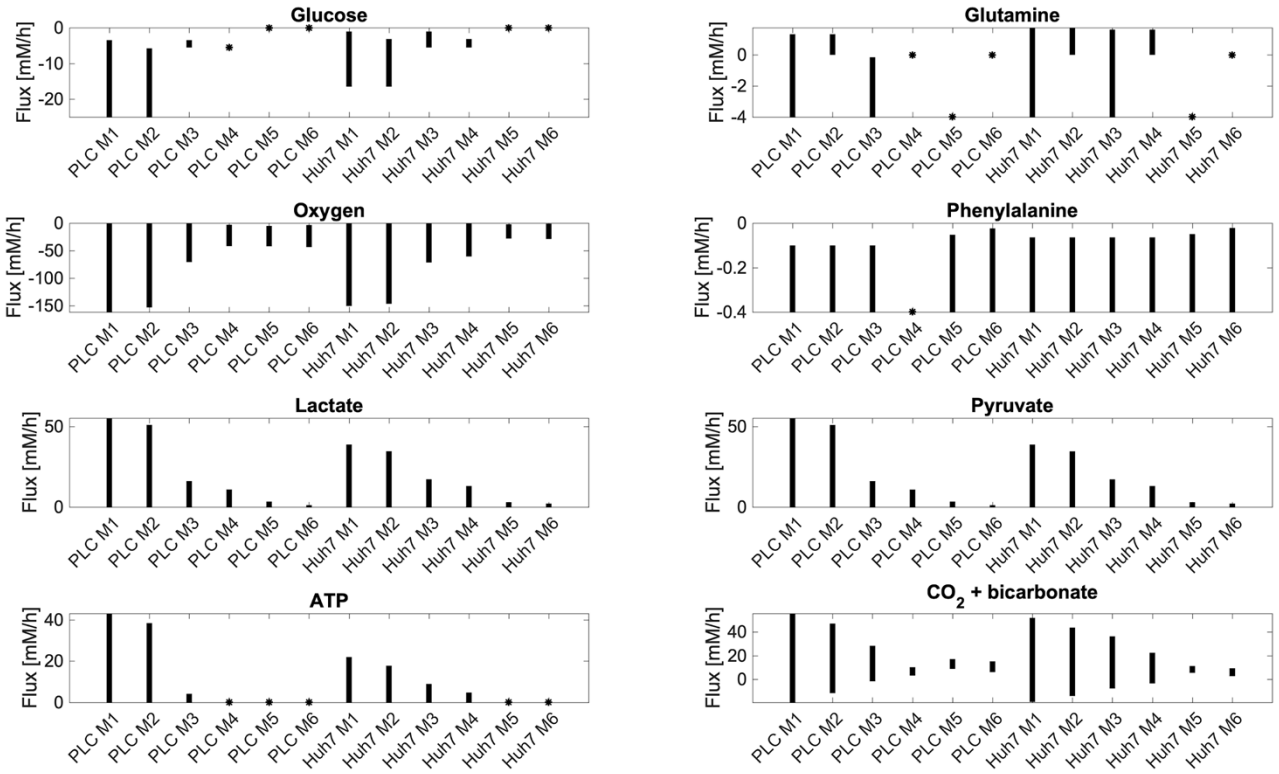

Figure 4. The range of uptake (if negative) / secretion (if positive) fluxes of various metabolites: computed to be consistent with maximal biomass flux and steady state. Uptake and secretion fluxes of metabolites have units of mM/h. Since we set maximal uptake fluxes equal to medium concentrations these rates differ from reality by some undetermined factor which is identical for all conditions. Minimal and maximal exchange fluxes for each of the compounds lactate, phenylalanine, glutamine, pyruvate, oxygen (O2) and CO_2 + bicarbonate and ATP hydrolysis flux (i.e. ATP + H_2O => ADP + P_i + H^+), were calculated using flux variability analysis [59] while requiring the model to produce the same maximum possible biomass fluxes shown in Figure 3. Maximal glucose and glutamine uptake fluxes had been set to their medium concentrations divided by 1 hour (see Table 1). In these calculations ATP is treated differently from the others. For the others the reaction was and remained present and potentially carrying varying flux when any of the yet other fluxes was manipulated in the FVA. For the ATP, the ATPase reaction was absent (no growth rate independent maintenance therefore) when doing FVA for any of the others and only present when ATP synthesis was manipulated by forcing flux through an ATP hydrolyzing added reaction. For visibility we used starred markers to indicate flux ranges with a width less than 0.1. These markers are typically located at minimal or maximal flux boundaries: e.g. zero glucose uptake in M5 and M6 or maximal phenylalanine uptake in PLC M4.

We further explored this by plotting some essential reactions for respiration to occur analogously to Figure 4 in terms of their minimal and maximal possible flux allowed while

bioRxiv preprint doi: https://doi.org/10.1101/674150; this version posted June 18, 2019. The copyright holder for this preprint (which was not certified by peer review) is the author/funder, who has granted bioRxiv a license to display the preprint in perpetuity. It is made available under aCC-BY 4.0 International license.

maintaining maximal biomass flux for the medium and cell type specified (Figure 5). In media with glucose the maximum growth rate does not require flux through cytochrome oxidase and oxidative phosphorylation with the exception of M4 for PLC. Figure 5 suggests that for PLC respiration in terms of flux through cytochrome oxidase is required for maintaining the maximal biomass flux in media 4-6 whereas for Huh7 this is required for media 5 and 6: rather than a range of fluxes, a precise non-zero flux magnitude is required. This suggest that only in those cases of limiting metabolic substrate, the maximal growth rate depends strictly on ATP produced by oxidative phosphorylation. This is in full agreement with the interpretation of the CO_2 + bicarbonate panel in Figure 4. In all other cases respiration is optional for maximum biomass synthesis flux, suggesting that the cells can obtain their ATP from other processes including aerobic glycolysis. To maintain their maximum growth rate at the 5.6 mM glucose concentration, they do need to use virtually all that glucose however (Figure 4).

Because of its assumptions of maintenance of maximum growth rate and full capability of the network to allow for various fluxes, flux variability analysis makes few predictions that may be put to the test in this study. Exceptions are (i) both cell lines should be capable of consuming the 5.6 or 25 mM glucose offered to them, (ii) they are not addicted to a 100% aerobic glycolysis, but can reduce lactate production without giving up their maximum growth rate, (iii) at glucose concentrations around 5 mM they would make use of all that glucose to grow maximally, (iv) They should be capable of catabolizing glutamine both in the absence and presence of glucose.

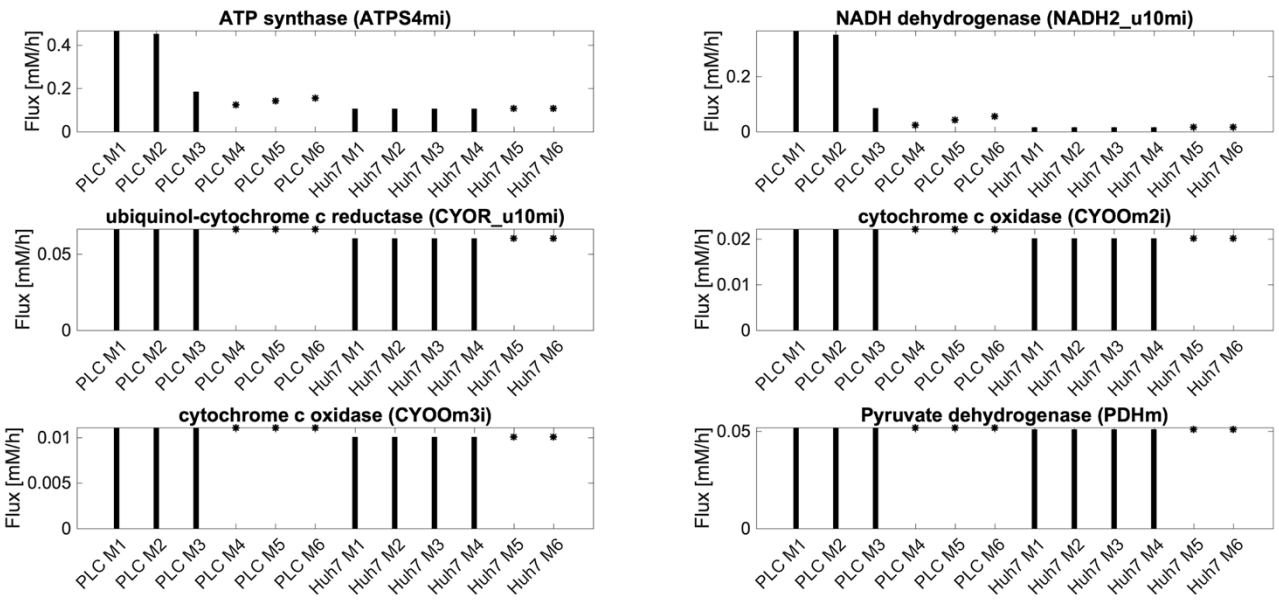

Figure 5. Range of allowed flux values through various reactions related to mitochondrial oxidative phosphorylation while maintaining the maximal biomass flux for the medium

bioRxiv preprint doi: https://doi.org/10.1101/674150; this version posted June 18, 2019. The copyright holder for this preprint (which was not certified by peer review) is the author/funder, who has granted bioRxiv a license to display the preprint in perpetuity. It is made available under aCC-BY 4.0 International license.

condition and cell type specified on the abscissa. See Table S3 for the detailed reactions. Uptake and secretion fluxes of metabolites have units of mM/h. Since we set maximal fluxes equal to medium concentrations (Table 1) these rates differ from reality by some factor.

3.3 *In vitro* experiments

3.3.1 Growth rate

In a first attempt to examine the applicability of our computational results, and to explore experimentally whether the concentrations of glucose and glutamine in the media control the cells proliferation rate, we evaluated the doubling time for Huh7 and PLC cell lines in six media containing different amounts of glucose and glutamine (see Figure 6A) for the first 24 h. We used DMEM media at 25, 5.6 and 0.0 mM concentration of glucose and 4.0 mM of glutamine (M1, M3, M5) and their counterparts without glutamine (M2, M4 and M6, respectively). In each of the six experimental conditions, the PLC cell line grew faster than the Huh7 cell line. In both HCC cell lines, the specific growth rate was almost the same for low and high glucose levels, 5.6 and 25 mM respectively. In the absence of glucose, cells grew more than 5 times more slowly. In the presence of glucose, the growth rate did not correlate with the level of glutamine in the medium, suggesting a lack of glutamine addiction in both cell lines. Only for media without glucose, the addition of glutamine to the growth medium led to a higher than 50% increase in the growth rate of both cell lines.

3.3.2 Glucose and glutamine consumption

During the same first 24 hours as when we measured growth rates, we observed a decrease in the concentration of glucose with time such that some 5 mM was consumed by the PLC cells (Figure 6B). In the PLC cultures that started with 5.6 mM glucose this resulted in almost full glucose depletion after the first day and night. In case of the Huh7 cell line, the consumption of glucose was higher in rich glucose medium than in low glucose medium reaching some 8.5 mM and 5 mM, respectively. Further velocity of glucose consumption for Huh7 was the same, while in case of PLC cells, after 24 h of culturing, stabilization appeared and lasted for next 20 hours (Figure 6B and 6C). We did not observe a difference in glucose consumption between media with and without glutamine. With respect to glutamine consumption by the cells we found that the level of glutamine did not change maintaining the 4.5 mM level for media with glutamine (that contained originally 4 mM) and 0.5 mM without.

bioRxiv preprint doi: https://doi.org/10.1101/674150; this version posted June 18, 2019. The copyright holder for this preprint (which was not certified by peer review) is the author/funder, who has granted bioRxiv a license to display the preprint in perpetuity. It is made available under aCC-BY 4.0 International license.

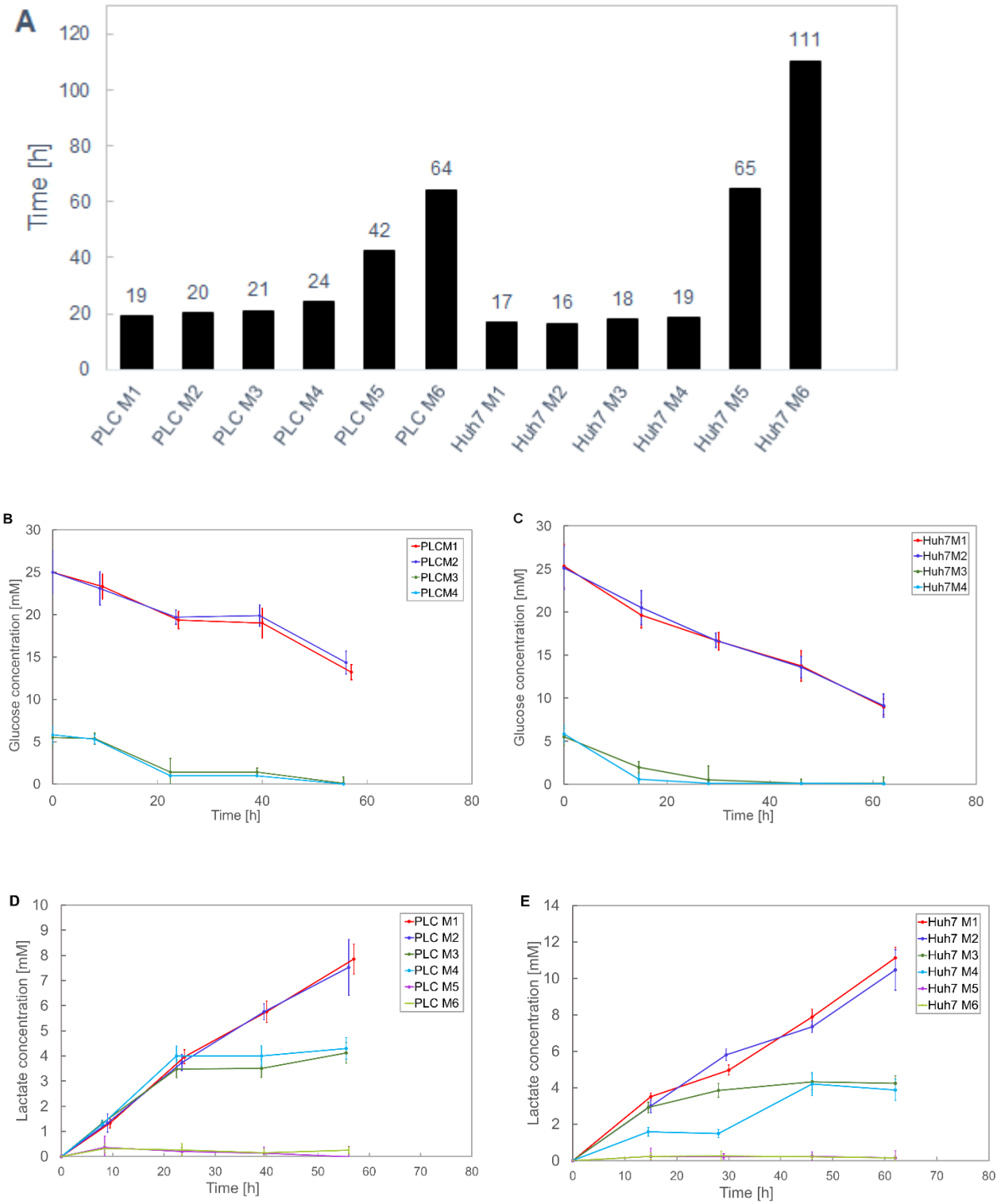

bioRxiv preprint doi: https://doi.org/10.1101/674150; this version posted June 18, 2019. The copyright holder for this preprint (which was not certified by peer review) is the author/funder, who has granted bioRxiv a license to display the preprint in perpetuity. It is made available under aCC-BY 4.0 International license.

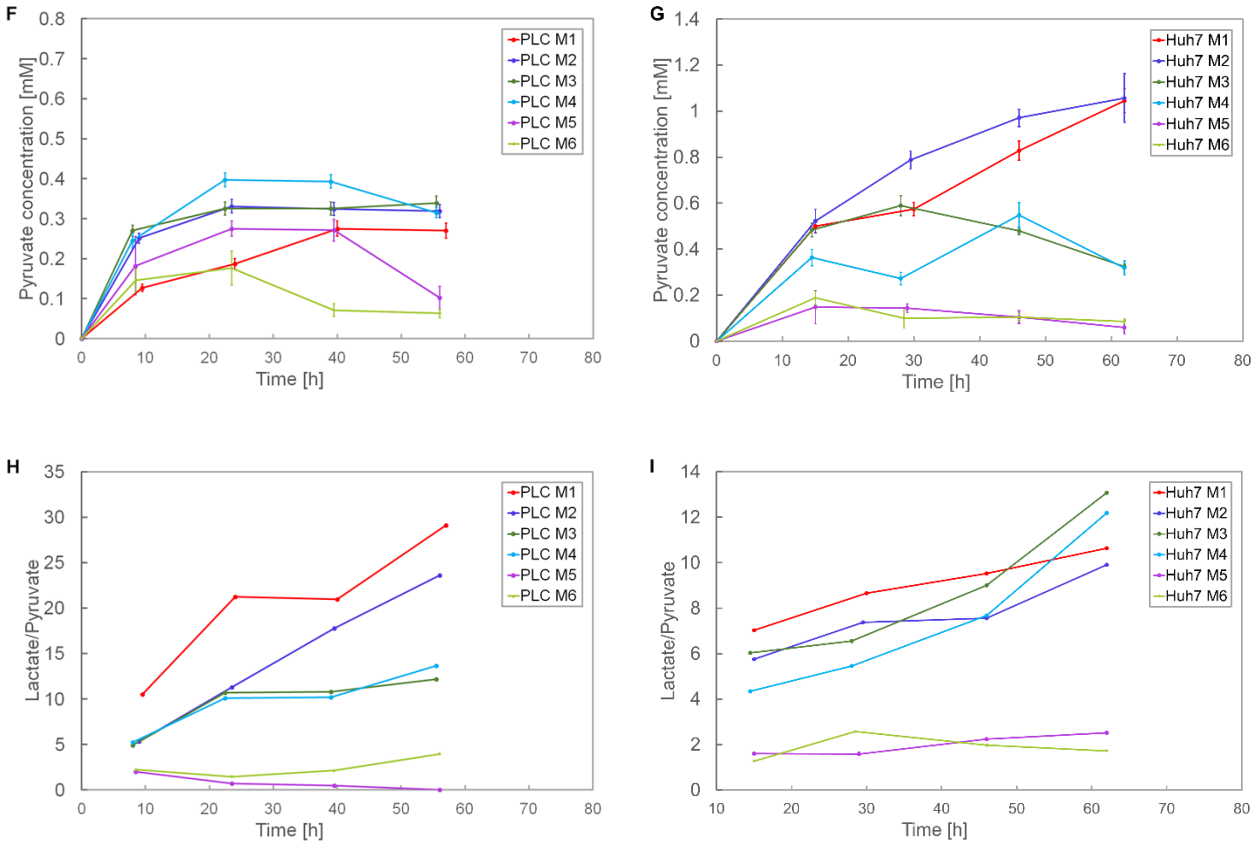

Figure 6. Metabolic performance as a function of time for Huh7 and PLC cells in six different media. (**A**) Biomass doubling time calculated based on a linear equation describing the variation of the number of the cells in the first 24h (see Figure S3 in SM). Glucose consumption by PLC (**B**) and Huh7 (**C**) in four different media. In media M5 and M6 glucose was not detected. Lactate production by PLC (**D**) and Huh7 (**E**) cells. Pyruvate secretion by PLC (**F**) and Huh7 (**G**) cells. Ratio of extracellular lactate to pyruvate in PLC (**H**) and Huh7 (**I**) cells starting from the second time point measured in panels D-G. In all six media the concentration of lactate and pyruvate before the experiments was 0 mM.

3.3.3 Lactate and pyruvate secretion

To gain additional insight into the dependence of the Warburg phenotype on cell nutritional shifts, we measured the production of lactate and pyruvate by cells using the same media conditions as above. In the case of the PLC cell line, the production of lactate was the same during the first 24 hours for M1 - M4, the lactate concentration reaching some 5 mM at the end of this time period. After 55 hours the concentration of lactate was twice higher in samples derived from the glucose-rich M1 and M2 (8.5 mM) than in samples taken from the low-glucose (5.6 mM) media M3 and M4, ostensibly because after 24 h the glucose had run out. In media low in glucose (M3 and M4), slightly over 40 % of the glucose was consumed during the experiment was transformed to lactate, while for M1 and M2 this was a bit less,

bioRxiv preprint doi: https://doi.org/10.1101/674150; this version posted June 18, 2019. The copyright holder for this preprint (which was not certified by peer review) is the author/funder, who has granted bioRxiv a license to display the preprint in perpetuity. It is made available under aCC-BY 4.0 International license.

i.e. 35% (Figure 7). For the Huh7 cells the trends were similar in case of M1 - M3 medium. In case of medium M4 such production was achieved only after 45 hours. In M1 and M2 lactate increased linearly with time attaining 10 mM at the end of experiment.

Pyruvate production was quite small for PLC cells, from 0.15 mM (M1 and M6) to 0.4 mM (M4) during the first 24 h. Pyruvate production was higher for media without glutamine (M2, M4 and M6 vs. M1, M3 and M5). For PLC cells, the lactate/pyruvate ratio (L/P) showed a positive relation with the glucose consumption, being highest for medium M1, and lowest for M5. For Huh7 cells, the timeseries for pyruvate (Figure 6G) look similar to those that show lactate secretion (Figure 6E). On M1-M4 the ratio of lactate to pyruvate changed over time from ~ 6 to ~10 whereas it stayed roughly constant for M5 and M6.

Consistent with the hypothesis that both cell lines exhibited a Warburg effect, they produced an amount of lactate proportionate to the amount of glucose that was present initially. Apparent differences merely derived from the glucose running out after some 30 h in the experiment starting at only 5.6 mM of glucose. Only part of the glucose was transformed to lactate, around ~43 % for low glucose media and perhaps a little as ~33 % in glucose-rich media. Thus, lactate production corresponded to only part of what might have been expected for full glucose conversion to lactate. This deficit in lactate secretion can be explained by the utilization of glucose for oxidative phosphorylation and as a source of carbon for the new biomass.

Consistently, we did not observe any difference between M1 and M2 for both cell lines nor did we observe such differences between M3 and M4 for PLC; for Huh7 small deviations were noticed. For the two cell lines we examined, this proves an independence of lactate production from glutamine access.

bioRxiv preprint doi: https://doi.org/10.1101/674150; this version posted June 18, 2019. The copyright holder for this preprint (which was not certified by peer review) is the author/funder, who has granted bioRxiv a license to display the preprint in perpetuity. It is made available under aCC-BY 4.0 International license.

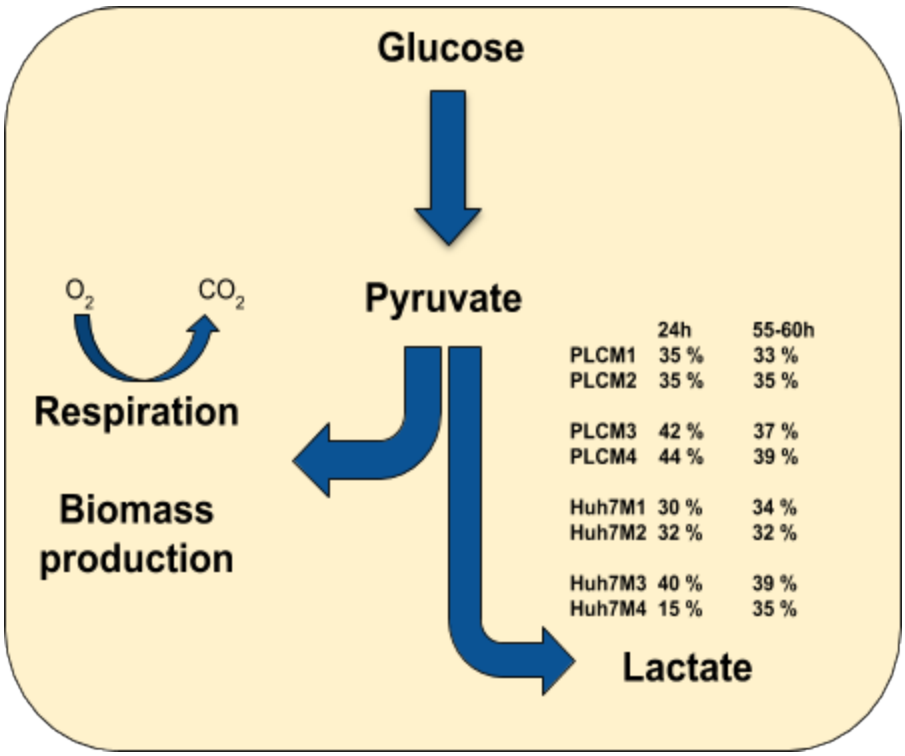

Figure 7. Schematic representation of branched glucose metabolism also indicating the percentage of the glucose carbon that was converted to lactate carbon in our experiments with glucose in the medium ($P = \Delta n_{lac} \div (2 \times \Delta n_{glu}) \times 100\%$). In the Warburg effect the percentage of glucose converted into and secreted as lactate is substantial even when there is sufficient oxygen for the glucose to be completely oxidized to carbon dioxide. For the maximal aerobic glucose fermentation, the value of P should be close to 100%, only deviating from that number because of carbon ending up in daughter cells. Values higher than the 100% minus the correction for growth rate, or values higher in glutamine containing media than in media without glutamine could reflect lactate production from glutamine, i.e. the WarburQ effect.

4. Discussion

Many human cancers including HCC produce lactate aerobically. This often correlates with tumor progression and worse clinical outcomes in cancer patients. Understanding how the Warburg effect is regulated in cancer and what nutrients are essential for tumor cells to survive, grow and divide may be relevant for identifying new therapeutic interventions. In this work we investigated the effect of two most suspected nutrients i.e. glucose and glutamine by way of six different medium conditions (see Table 1 and 2) using both computational and experimental approaches.

bioRxiv preprint doi: https://doi.org/10.1101/674150; this version posted June 18, 2019. The copyright holder for this preprint (which was not certified by peer review) is the author/funder, who has granted bioRxiv a license to display the preprint in perpetuity. It is made available under aCC-BY 4.0 International license.

In order to perform the *in silico* analysis we elaborated a new method to generate models based on the latest human metabolic map (i.e. Recon3D [37]) that take transcriptomic data as well as different medium conditions into account. We thereby obtained twelve (six for PLC and six for Huh7) models that integrate transcriptomic (*nature*) and nutrient concentration (*nurture*) data through a new FBA approach, by using proposed by us a new NNS factor. Our new methodology enabled us to predict metabolic changes upon nutrition shift by flux balance analysis.

In this work, we studied the Warburg effect per se. We therefore selected cell types that do exhibit the Warburg effect clearly. We used transcriptomic data from the cell population in its entirely and the models are a representation thereof. Single cell transcriptomic studies suggest that cancer cell populations are heterogeneous, but single cell metabolomics does not yet enable us to examine the consequences for metabolism. Thus, we assumed in model that the cell population was homogeneous.

Our findings offer support for the predictive potential of genome-scale metabolic maps together with transcriptomic data sets and nutrients composition. The predictions address the carbon and energy metabolism of cancer cells. Because much of this metabolism is essential for cell survival, the potential may translate to new drug targets in a long-neglected area of drug discovery. Indeed, we have shown that dependencies on medium composition and gene expression can be computed and that the results are then relevant enough to be compared with experimental work. Moreover, in most cases the predictions were matched by the experimental results.

Notwithstanding these successes, our methodology comes with a number of issues. One of these relates to whether expression level information was properly translated to flux. In contrast to several methods developed to extract context-specific models [60-62] that focused on threshold selection with exception of some essential metabolic functions that are needed for cell growth, our method used a linear relationship between flux bounds and the transcriptome. Such a linear approach was first proposed by Colijn *et al.* [55] and applied in the MaREA framework by Graudenzi et al. [54], where it was shown to be of use in comparing the metabolism of samples in distinct subgroups. The approach assumes that the V_{max} of a reaction is proportional to the level of the mRNA encoding the enzyme, with a proportionality constant equal for all reactions. It thereby neglects differential translation and posttranslational regulation, and assumes all k_{cat} to be equal. Both assumptions are often far from the truth but have the advantage that they can be improved upon in the future by consulting more literature information for the steps that turn out to be important. Keeping the transcriptomics data the same as in the literature source, we were further assuming that

bioRxiv preprint doi: https://doi.org/10.1101/674150; this version posted June 18, 2019. The copyright holder for this preprint (which was not certified by peer review) is the author/funder, who has granted bioRxiv a license to display the preprint in perpetuity. It is made available under aCC-BY 4.0 International license.

the transcriptome remained constant at the time scale of 12 hours that essentially determined our results; we propose that a single cell cycle or less (i.e. < 24 hours) should qualify for this assumption. Furthermore, we assume that the cell lines in our experiments have not significantly evolved compared to those used in the transcriptomics datasets [46]. We did not take into consideration epigenetic and gene-expression changes that could occur during culturing. In addition, our approach equated concentrations of medium components with exchange reaction bounds, again treating all compounds equally. The limitations of this step include the failure to take into consideration the kinetics and expression levels of transporters. What is also peculiar in our approach is the arbitrary magnitude of the ratio of the proportionality constant relating mRNA level to enzyme bound to the proportionality constant relating medium concentration to exchange bound. We mediated this problem somewhat by setting the NNS factor to a value that enabled the models to shift form limitation by medium concentration to limitation by expression level. Here an additional issue is that the effect a given value of α has on model output fundamentally depends on the medium definition, since on different media a different NNS value might be needed to affect the objective value or produce a certain metabolic behavior. On top of this, there are the generic limitations of flux balance analysis that come with the assumption that cells 'know' how to arrange their metabolism so as to be optimal for maximal growth rate, even in case of perhaps new perturbations. A further limitation to our approach lies in the constancy assumed in the medium concentrations. As a metabolic steady state is attained at a faster time scale than the change in extracellular metabolite concentrations, one may simulate the physiological changes in glucose and lactate levels in the body by using a model of the type presented here. All these issues require further substantiation or substitution with better assumptions or data. The results of this study should thereby be classified as a proof of the principle that it should become possible to integrate transcriptome and medium composition data into metabolic-map based flux-balance analysis.

Indeed, despite all these issues and limitations, we have succeeded in computing dependencies on medium composition and gene expression that did make sense experimentally. *In silico* experiments showed that the specific growth rate of Huh7 cells is lower than that of PLC cells, which was also observed during *in vitro* experiments on these cell lines. Given the positive correlation between the *in silico* biomass flux and the experimentally determined growth rate we speculated that the *in silico* results pertaining to the range of uptake and secretion fluxes of various metabolites might also correlate with experimental results. Modelling showed that in the absence and in the presence of glutamine the growth rate should be independent of glucose concentrations between 5.6 and 25 mM.

bioRxiv preprint doi: https://doi.org/10.1101/674150; this version posted June 18, 2019. The copyright holder for this preprint (which was not certified by peer review) is the author/funder, who has granted bioRxiv a license to display the preprint in perpetuity. It is made available under aCC-BY 4.0 International license.

This apparent V_{max} effect is of conceptual interest because it does not derive from the kinetics of any enzyme or transporter, but from a shift between the exchange or the metabolism bound being hit by the flux. Also, experimentally the growth rate reached the same level for four medium conditions (M1-M4) that contained 5.6 and 25 mM of glucose for both HCC cell lines. Moreover, both approaches, computational and experimental, showed that in the absence of glucose, the cells should be able to grow on glutamine but with a much lower growth rate than on glucose alone.

According to the flux variability analysis predictions both cell lines should have a higher potential; they should be capable of consuming the 5.6 or 25 mM glucose offered to them. Yet, our *in vitro* observations indicated that PLC cells confronted with the 25 mM did not consume more than the around 5 mM during the first 24 hours. They did not make use of that full potential. We conclude that there is a maximum amount of glucose per unit time that the cells 'wish to' handle at glucose levels above a few mM, because other issues than energy and carbon may limit the cells' growth. We use the term 'wish to' to indicate that this may be an issue of metabolic regulation: the gene expression would allow for higher glucose uptake fluxes.

The cells that had consumed in the first 24 h some 5 mM of the 5.6 mM glucose they had been incubated with, continued to grow for the next 24 hours at virtually the same growth rate; they must have done this at a much-reduced glucose consumption rate. Since they also stopped producing lactate, we suspect that the small amount (approximately 0.5 mM) of glucose left provided the cells with sufficient ATP to drive their continued growth. The cells may have reverted from lactate production to respiration with its more than 15-fold higher ATP yield. This highlights that there may be a limitation to these cells' addiction to lactate production: these cancer cells can shift to glucose oxidation. We observed a slightly different effect in the case of the Huh7 cell line: the consumption of glucose was almost two times higher in rich glucose medium (25 mM) than low on (5 mM) during the first 24 hours. *In silico* analyses predicted and *in vitro* experiments confirmed that both cell lines, at glucose concentrations around 5 mM, made use of all available glucose to grow maximally. They also showed that upon glucose depletion and if asked to grow at maximal growth rate, the cells should shift to glucose respiration (Figure 4 and 5).

Lactate production correlated with glucose consumption. Between 15% and 44% of the glucose was transformed to lactate during first 24 hours. Partially contrary to the predictions by our Flux Balance Analysis, we did not detect consumption of glutamine in any medium and for either cell line in the experimental work: the glutamine concentration was constant through all time points, maintaining the 4.5 mM level for media with extra glutamine

bioRxiv preprint doi: https://doi.org/10.1101/674150; this version posted June 18, 2019. The copyright holder for this preprint (which was not certified by peer review) is the author/funder, who has granted bioRxiv a license to display the preprint in perpetuity. It is made available under aCC-BY 4.0 International license.

(4 mM) and 0.5 mM for the media without, even though in absence of glucose from the medium, the cells grew faster when they did have access to glutamine. This observation was in contrast with the modelling results according to which, the cell lines should be capable of catabolizing glutamine both in the absence and presence of glucose. According to the computational experiments, glutamine consumption should have been required to achieve optimal growth in medium 3 for PLC and in medium 5 for both PLC and Huh7 cells. Here the limitation of FBA that it requires an objective function, such as the assumption that the cells have been reprogrammed to provide a maximal growth rate, may be at fault.

Under aerobic conditions, 'social' cells use mitochondria to oxidize the glycolysis-derived pyruvate. In the absence of oxygen however, they ferment glucose into lactate. The phenomenon of aerobic lactate production from glucose has been termed the Warburg effect and is characteristic of many fast-growing cancer cells [10,12,62-65]. DeBerardinis et al. [66] examined the metabolism of glioblastoma cells exhibiting aerobic glycolysis where the cells were incubated under oxygenated conditions in 10 mM C-13-labelled glucose and then provided with 4 mM C-12 glucose prior to metabolomics analysis. High levels of C-12 glycolytic metabolites were observed in line with the Warburg effect. In the same study, a high rate of glutamine consumption was observed that could not be explained by the nitrogen demand imposed by nucleotide synthesis or maintenance of nonessential amino acid pools. Most cancer cells have active and functional mitochondria, contrary to Warburg's original hypothesis for the mechanism of the Warburg effect [67,68]. Weinhouse et al. reported that slow-growing rat hepatoma cells were more oxidative, whereas the more proliferative hepatomas were more fermentative [69]. Zu and Guppy reported that ATP derived through aerobic lactate production in various cancers and cell lines accounts for only 17% of the total ATP [70], still more however than the expected 5% expected for equal lactate production and respiration.

While the involvement of glucose in cancer cell metabolism has been widely studied [10,62,63,71], most such cancer cells were grown on cell culture media containing high levels of glucose, i.e. between 10 and 25 mM [72], and without addressing glutamine utilization. Many cancer cell lines, including some of the Warburg type, display addiction to glutamine [23,27] with some dying rapidly if they are deprived of glutamine. But there are also cancer cells that are not addicted to glutamine [66].

The next question that remains to be addressed relates to the heterogeneity of population and the Intracellular Lactate Shuttle [10b,12b]. Future investigations with single cell transcriptomic/metabolomic data and multi-cells genome scale model are warranted to address this question.

bioRxiv preprint doi: https://doi.org/10.1101/674150; this version posted June 18, 2019. The copyright holder for this preprint (which was not certified by peer review) is the author/funder, who has granted bioRxiv a license to display the preprint in perpetuity. It is made available under aCC-BY 4.0 International license.

In summary, our novel approach that integrates *nature* (the expression level) and *nurture* (the environment), let us to corelate proliferation, glucose consumption, and lactate production with the medium concentrations of glucose and glutamine. Our findings delineate a limitation of glucose consumption by HCC cells. Their growth rate was completely independent of glutamine in case of media containing glucose. In view of the requirement of nitrogen for biomass synthesis, this reflects the importance of gratuitous components of growth media. We show that even under typical physiologically relevant conditions, where plasma glucose lies between 4 and 6 mM, production of lactate occurs pointing to aerobic glycolysis. Our results suggest that only a reduction of blood glucose levels to below 5 mM may result in decreased cancer cell proliferation. This conclusion is supported by recent research where Metformin (a drug that decreases blood glucose levels mainly by suppressing liver glucose production through gluconeogenesis) turned out to be more effective in enhancing chemotherapy sensitivity of cancer cells under reduced glucose conditions [72].

Author Contributions

EWT formulated the problem, proposed and designed the project, with advice from HVW. EWT conceived the strategy of the study with contributions from TDM and HVW. EWT designed *in vitro* experimental work that was performed by EWT and DP. Computational analyses were designed and performed by TDM with advice from EWT and HVW and interpreted by TDM, EWT and HVW. EWT, TDM and HVW wrote the manuscript.

Conflicts of Interest

The authors declare that there is no conflict of interest.

Acknowledgments

This work is co-supported by the research Priority Area of the University of Amsterdam. EWT is financed by a grant Mobilność Plus V from the Polish Ministry of Science and Higher Education (Grant No. 1639/MOB/V/2017/0). HVW received funding from various grants: Corbel: EU-H2020 (NFRADEV-4-2014-2015 #654248) and Epipredict: EU-H2020 MSCA-ITN-2014-ETN: Marie Skłodowska-Curie Innovative Training Networks (ITN-ETN) #642691. The funders had no role in study design, data collection and analysis, decision to publish, or preparation of the manuscript.

We gratefully acknowledge Eugenie Troia and Hugo Pineda Hernández for their kind help with HPLC and Stefania Astrologo for pointing out the existing datasets and for assistance

bioRxiv preprint doi: https://doi.org/10.1101/674150; this version posted June 18, 2019. The copyright holder for this preprint (which was not certified by peer review) is the author/funder, who has granted bioRxiv a license to display the preprint in perpetuity. It is made available under aCC-BY 4.0 International license.

with early modeling work. We thank Chiara Damiani for discussing possible extensions of the MaREA methodology, inspiring us to the implementation here.

Supplementary Files

- Supplementary material
- Supplementary Excel Table 1: Recon3D.01 (Adjusted according to Methods section)
- Supplementary Excel Table 2: List of metabolites that may be secreted
- Supplementary Excel Table 3: Reactions with a RAS fold-change of at least 100
- All Python and MATLAB code, Jupyter Notebooks and raw data files are available as part of a Github repository https://github.com/ThierryMondeel/HCC_flux_balance_analysis

References

1. Balogh J, Victor D 3rd, Asham EH, Burroughs SG, Boktour M et al. Hepatocellular carcinoma: a review. J Hepatocell Carcinoma. 2016; 3: 41-53.

2. Bertuccio P, Turati F, Carioli G, Rodriguez T, La Vecchia C et al. Global trends and predictions in hepatocellular carcinoma mortality. J Hepatol; 2017; 67(2): 302-309.
doi: 10.2147/JHC.S61146

3. Ferlay J, Parkin DM, Steliarova-Foucher E. Estimates of cancer incidence and mortality in Europe in 2008. Eur J Cancer. 2010; 46: 765-781.

4. El-Serag HB, Rudolph KL. Hepatocellular carcinoma: epidemiology and molecular carcinogenesis. Gastroenterology. 2007; 132(7): 2557-2576.
doi: 10.1053/j.gastro.2007.04.061

5. Ghouri YA, Mian I, Rowe JH. Review of hepatocellular carcinoma: Epidemiology, etiology, and carcinogenesis. J Carcinog. 2017; 16: 1.
doi: 10.4103/jcar.JCar_9_16.

6. Arzumanyan A, Reis H, Feitelson MA. Pathogenic mechanisms in HBV- and HCV-associated hepatocellular carcinoma. Nat Rev Cancer. 2013; 13: 123-135.
doi: 10.1038/nrc3449.

7. Cauchy F, Fuks D, Belghiti J. HCC: Current surgical treatment concepts. Langenbeck Arch Surg. 2012; 397: 681-695.
doi: 10.1007/s00423-012-0911-2.

8. https://seer.cancer.gov/statfacts/html/livibd.html

bioRxiv preprint doi: https://doi.org/10.1101/674150; this version posted June 18, 2019. The copyright holder for this preprint (which was not certified by peer review) is the author/funder, who has granted bioRxiv a license to display the preprint in perpetuity. It is made available under aCC-BY 4.0 International license.

9. DeBerardinis RJ, Chandel NS. Fundamentals of cancer metabolism. Sci Adv. 2016; 2, e1600200.
doi: 10.1126/sciadv.1600200.

10. (a) Liberti MV, Locasale JW. The Warburg Effect: How Does it Benefit Cancer Cells? Trends Biochem Sci. 2016; 41, 211-218.
doi: 10.1016/j.tibs.2015.12.001.

10. (b) San-Millán I, Brooks GA. Reexamining cancer metabolism: lactate production for carcinogenesis could be the purpose and explanation of the Warburg Effect. Carcinogenesis. 2017; 38(2) :119-133.
doi: 10.1093/carcin/bgw127.

11. Gatenby RA, Gillies RJ. Why do cancers have high aerobic glycolysis? Nat Rev Cancer. 2004; 4(11): 891-899.
doi: 10.1038/nrc1478.

12. (a) Warburg O. üeber den Stoffwechsel der Tumoren. Biochem Z. 1923; 152: 319-344.
doi: 10.1158/jcr.1925.148

12. (b) Racker E. Bioenergetics and the problem of tumor growth. Am Sci. 1972; 60(1): 56-63.

13. Kitamura K, Hatano E, Higashi T, Narita M, Seo S et al. Proliferative activity in hepatocellular carcinoma is closely correlated with glucose metabolism but not angiogenesis. J Hepatol. 2011; 55(4): 846-857.
doi: 10.1016/j.jhep.2011.01.038.

14. Iansante V, Choy PM, Fung SW, Liu Y, Chai JG et al. PARP14 promotes the Warburg effect in hepatocellular carcinoma by inhibiting JNK1-dependent PKM2 phosphorylation and activation. Nat Commun. 2015; 6: 7882.
doi: 10.1038/ncomms8882.

15. Vaughn AE, Deshmukh M. Glucose metabolism inhibits apoptosis in neurons and cancer cells by redox inactivation of cytochrome c. Nat Cell Biol. 2008; 10(12): 1477-1483.
doi: 10.1038/ncb1807.

16. Gui DY, Lewis CA, Vander Heiden MG. Allosteric regulation of PKM2 allows cellular adaptation to different physiological states. Sci Signal. 2013; 6(263): pe7.
doi: 10.1126/scisignal.2003925.

17. Romero-Garcia S, Moreno-Altamirano MMB, Prado-Garcia H, Sánchez-García FJ. Lactate contribution to the tumor microenvironment: mechanisms, effects on immune cells and therapeutic relevance. Front Immunol. 2016; 7: 52.
doi: 10.3389/fimmu.2016.00052.

bioRxiv preprint doi: https://doi.org/10.1101/674150; this version posted June 18, 2019. The copyright holder for this preprint (which was not certified by peer review) is the author/funder, who has granted bioRxiv a license to display the preprint in perpetuity. It is made available under aCC-BY 4.0 International license.

18. Lu J, Tan M, Cai Q. The Warburg effect in tumor progression: mitochondrial oxidative metabolism as an anti-metastasis mechanism. Cancer Lett. 2015; 356 (2 Pt A): 156-164.
doi: 10.1016/j.canlet.2014.04.001.

19. Beyoğlu D, Imbeaud S, Maurhofer O, Bioulac-Sage P, Zucman-Rossi J et al. Tissue metabolomics of hepatocellular carcinoma: tumor energy metabolism and the role of transcriptomic classification. Hepatology. 2013; 58(1): 229-238.
doi: 10.1002/hep.26350.

20. Beyoğlu D, Idle JR. The metabolomic window into hepatobiliary disease. J Hepatol. 2013; 59(4): 842-858. doi: 10.1016/j.jhep.2013.05.030.

21. Nwosu ZC, Megger DA, Hammad S, Sitek B, Roessler S et al. Identification of the consistently altered metabolic targets in human hepatocellular carcinoma. Cell Mol Gastroenterol Hepatol. 2017; 4(2): 303-323.e1.
doi: 10.1016/j.jcmgh.2017.05.004.

22. DeBerardinis RJ, Mancuso A, Daikhin E, Nissim I, Yudkoff M et al. Beyond aerobic glycolysis: transformed cells can engage in glutamine metabolism that exceeds the requirement for protein and nucleotide synthesis. Proc Natl Acad Sci USA. 2007; 104(49): 19345-19350.
doi: 10.1073/pnas.0709747104.

23. Altman BJ, Stine ZE, Dang CV. From Krebs to clinic: glutamine metabolism to cancer therapy. Nat Rev Cancer. 2016; 16(10): 619-634.
doi: 10.1038/nrc.2016.71.

24. Cluntun AA, Lukey MJ, Cerione RA, Locasale JW. Glutamine Metabolism in Cancer: Understanding the Heterogeneity. Trends Cancer. 2017; 3(3): 169-180.
doi: 10.1016/j.trecan.2017.01.005.

25. Hensley CT, Wasti AT, DeBerardinis RJ. Glutamine and cancer: cell biology, physiology, and clinical opportunities. J Clin Invest. 2013; 123(9): 3678-3684.
doi: 10.1172/JCI69600.

26. Wise DR, Thompson CB. Glutamine addiction: a new therapeutic target in cancer. Trends Biochem. 2010; 35: 427-433.

27. Damiani C, Colombo R, Gaglio D, Mastroianni F, Pescini D, Westerhoff HV, Mauri G, Vanoni M, Alberghina LA. metabolic core model elucidates how enhanced utilization of glucose and glutamine, with enhanced glutamine-dependent lactate production, promotes cancer cell growth: The WarburQ effect. PLoS Comput Biol. 2017; 13: e1005758.
doi: 10.1371/journal.pcbi.1005758.

bioRxiv preprint doi: https://doi.org/10.1101/674150; this version posted June 18, 2019. The copyright holder for this preprint (which was not certified by peer review) is the author/funder, who has granted bioRxiv a license to display the preprint in perpetuity. It is made available under aCC-BY 4.0 International license.

28. Adeva-Andany M, López-Ojén M, Funcasta-Calderón R, Ameneiros-Rodríguez E, Donapetry-García C et al. Comprehensive review on lactate metabolism in human health. Mitochondrion. 2014;17: 76-100.
doi: 10.1016/j.mito.2014.05.007.

29. Gebhardt R, Baldysiak-Figiel A, Krügel V, Ueberham E, Gaunitz F.Hepatocellular expression of glutamine synthetase: an indicator of morphogen actions as master regulators of zonation in adult liver. Prog Histochem Cytochem. 2007; 41(4): 201-266.
doi: 10.1016/j.proghi.2006.12.001.

30. Long J, Wang H, Lang Z, Wang T, Long M et al. Expression level of glutamine synthetase is increased in hepatocellular carcinoma and liver tissue with cirrhosis and chronic hepatitis B. Hepatol Int. 2011; 5(2): 698-706.
doi: 10.1007/s12072-010-9230-2.

31. Brooks GA. Cell Metab. 2018; 27(4): 757-785.
doi: 10.1016/j.cmet.2018.03.008.

32. Ferguson BS, Rogatzki MJ, Goodwin ML, Kane DA, Rightmire Z, Gladden LB. Lactate metabolism: historical context, prior misinterpretations, and current understanding. Eur J Appl Physiol. 2018; 18(4): 691-728.
doi: 10.1007/s00421-017-3795-6.

33. Brooks GA. Cell-cell and intracellular lactate shuttles. J Physiol. 2009; 587(Pt 23): 5591-600.
doi: 10.1113/jphysiol.2009.178350.

34. Ma R, Zhang W, Tang K, Zhang H, Zhang Y et al. Switch of glycolysis to gluconeogenesis by dexamethasone for treatment of hepatocarcinoma. Nat Commun. 2013; 4: 2508.
doi: 10.1038/ncomms3508

35.Duarte NC, Becker SA, Jamshidi N, Thiele I, Mo M. L et al. Global reconstruction of the human metabolic network based on genomic and bibliomic data. Proc Natl Acad Sci U S A. 2007; 104(6): 1777-1782.

36. Thiele I, Swainston N, Fleming R M, Hoppe A, Sahoo S, Aurich MK, et al. A community-driven global reconstruction of human metabolism. Nat Biotechnol. 2013; 31(5): 419-425.
doi: 10.1038/nbt.248837.

37. Brunk E, Sahoo S, Zielinski DC, Altunkaya A, Dräger A et al. Recon3D enables a three-dimensional view of gene variation in human metabolism. Nat Biotechnol. 2018; 36(3): 272-281.
doi: 10.1038/nbt.4072.

bioRxiv preprint doi: https://doi.org/10.1101/674150; this version posted June 18, 2019. The copyright holder for this preprint (which was not certified by peer review) is the author/funder, who has granted bioRxiv a license to display the preprint in perpetuity. It is made available under aCC-BY 4.0 International license.

38. Shlomi T, Cabili M, Ruppin E. Predicting metabolic biomarkers of human inborn errors of metabolism. Mol Syst Biol. 2009; 5: 263.
doi: 10.1038/msb.2009.

39. Frezza C, Zheng L, Folger O, Rajagopalan KN, MacKenzie ED, Jerby L, et al. Haem oxygenase is synthetically lethal with the tumour suppressor fumarate hydratase. Nature. 2011; 477: 225-228.

40. Damiani C Maspero D, Di Filippo M Colombo R, Pescini D, Graudenzi A, Westerhoff HV, Alberghina L, Vanoni M, Mauri G. Integration of single-cell RNA-seq data into population models to characterize cancer metabolism. PLoS Comput Biol. 2019; 15(2): e1006733.
doi: 10.1371/journal.pcbi.1006733.

41. Sen P, Orešič M. Metabolic Modeling of Human Gut Microbiota on a Genome Scale: An Overview. Metabolites. 2019; 9(2). pii: E22.doi: 10.3390/metabo9020022.

42. Heinken A, Thiele I. Systematic prediction of health-relevant human-microbial co-metabolism through a computational framework. Gut Microbes. 2015; 6, 120–130.

43. Daemer RJ, Feinstone SM, Alexander JJ, Tully JG, London WT et al. PLC/PRF/5 (Alexander) hepatoma cell line: further characterization and studies of infectivity. Infect Immun. 1980; 30(2): 607-611.

44. Krelle AC, Okoli AS, Mendz GL. Huh-7 Human Liver Cancer Cells: A Model System to Understand Hepatocellular Carcinoma and Therapy. JCT. 2013; 4: 606-631.
doi: 10.4236/jct.2013.42078.

45. Shaul YD, Yuan B, Thiru P, Nutter-Upham A, McCallum S et al. MERAV: a tool for comparing gene expression across human tissues and cell types. Nucleic Acids Res. 2016; 44(D1): D560-D566.
doi: 10.1093/nar/gkv1337.

46. Ma MKF, Lau EYT, Leung DHW, Lo J, Ho NPY et al. Stearoyl-CoA desaturase regulates sorafenib resistance via modulation of ER stress-induced differentiation. J Hepatol. 2017; 67(5): 979-990.
doi: 10.1016/j.jhep.2017.06.015.

47. Orth JD, Thiele I, Palsson BØ. What is flux balance analysis? Nat Biotechnol. 2010; 28(3): 245-248.
doi: 10.1038/nbt.1614.

48. Heirendt L, Arreckx S, Pfau T, Mendoza SN, Richelle A et al. Creation and analysis of biochemical constraint-based models: the COBRA Toolbox v3.0 Nat Protoc. 2019; 14(3): 639-702.
doi: 10.1038/s41596-018-0098-2.49.

bioRxiv preprint doi: https://doi.org/10.1101/674150; this version posted June 18, 2019. The copyright holder for this preprint (which was not certified by peer review) is the author/funder, who has granted bioRxiv a license to display the preprint in perpetuity. It is made available under aCC-BY 4.0 International license.

49. Ebrahim A, Lerman JA, Palsson BO, Hyduke DR. COBRApy: COnstraints-Based Reconstruction and Analysis for Python. BMC Systems Biology. 2013; 7(1): 74.
doi: 10.1186/1752-0509-7-74

50. Place TL, Domann FE, Case A J. Limitations of oxygen delivery to cells in culture: An underappreciated problem in basic and translational research. Free Radic Biol Med. 2017; 113: 311-322.

51. Krab K, Kempe H. Wikström M. Explaining the enigmatic KM for oxygen in cytochrome c oxidase: A kinetic model. Biochim Biophys Acta. 2011; 1807(3): 348-358.
doi: 10.1016/j.bbabio.2010.12.015.

52. Swainston N, Smallbone K, Hefzi H, Dobson PD, Brewer J et al. Recon 2.2: from reconstruction to model of human metabolism. Metabolomics. 2016; 12(7): 109.
doi: 10.1007/s11306-016-1051-4.

53. Hicks SC, Townes FW, TengM, Irizarry RA.Missing data and technical variability in single-cell RNA-sequencing experiments. Biostatistics 2018; 19(4): 562-578.
doi: 10.1093/biostatistics/kxx053.

54. Graudenzi A, Maspero D, Di Filippo M, Gnugnoli M, Isella C et al. Integration of transcriptomic data and metabolic networks in cancer samples reveals highly significant prognostic power. J Biomed Inform. 2018; 87, 37-49.
doi: 10.1016/j.jbi.2018.09.010.

55. Colijn C, Brandes A, Zucker J, Lun DS, Weiner B et al. Interpreting expression data with metabolic flux models: Predicting Mycobacterium tuberculosis mycolic acid production. PLoS Comput Biol. 2009; 5(8): e1000489.
doi: 10.1371/journal.pcbi.1000489.

56. Rybakova KN, Bruggeman FJ, Tomaszewska A, Moné MJ, Carlberg C et al. Multiplex Eukaryotic Transcription (In)activation: Timing, Bursting and Cycling of a Ratchet Clock Mechanism. PLoS Comput Biol. 2015; 11(4): e1004236.
doi: 10.1371/journal.pcbi.1004236.

57. ter Kuile BH, Westerhoff HV. Transcriptome meets metabolome: hierarchical and metabolic regulation of the glycolytic pathway. FEBS Lett. 2001; 500(3): 169-171.
doi: 10.1016/S0014-5793(01)02613-8.

58. Smallbone K, Messiha HL, Carroll KM, Winder CL, Malys N et al. A model of yeast glycolysis based on a consistent kinetic characterisation of all its enzymes. FEBS Lett. 2013; 587(17): 2832-2841.
doi: 10.1016/j.febslet.2013.06.043.

bioRxiv preprint doi: https://doi.org/10.1101/674150; this version posted June 18, 2019. The copyright holder for this preprint (which was not certified by peer review) is the author/funder, who has granted bioRxiv a license to display the preprint in perpetuity. It is made available under aCC-BY 4.0 International license.

59. Mahadevan R, Schilling CH. The effects of alternate optimal solutions in constraint-based genome-scale metabolic models. Metab Eng. 2003; 5(4): 264-276.
doi: 10.1016/j.ymben.2003.09.002.

60. Opdam S, Richelle A, Kellman B, Li S, Zielinski DC et al. A Systematic Evaluation of Methods for Tailoring Genome-Scale Metabolic Models. Cell Syst. 2017; 4(3): 318-329.e6.
doi: 10.1016/j.cels.2017.01.010.

61. Agren R, Mardinoglu A, Asplund A, Kampf C, Uhlen M, Nielsen. Identification of anticancer drugs for hepatocellular carcinoma through personalized genome-scale metabolic modeling. J Mol Syst Biol. 2014; 10: 721.
doi: 10.1002/msb.145122.

62. Vlassis N, Pacheco MP, Sauter T. Fast reconstruction of compact context-specific metabolic network models. PLoS Comput Biol. 2014; 10: e1003424.
doi: 10.1371/journal.pcbi.1003424.

63. Warburg O, Posener K, Negelein E. Ueber den stoffwechsel der tumoren. Biochemische Zeitschrift. 1924; 152(1): 319-344.

64. Warburg O, Wind F, Negelein E. The metabolism of tumors in the body. The Journal of general physiology. 1927; 8(6): 519-530.

65. Vander Heiden MG, Cantley LC, Thompson CB. Understanding the Warburg effect: the metabolic requirements of cell proliferation. Science. 2009; 324, 1029-1033.
doi: 10.1126/science.1160809.

66. DeBerardinis RJ1, Lum JJ, Hatzivassiliou G, Thompson CB. The biology of cancer: metabolic reprogramming fuels cell growth and proliferation. Cell Metab. 2008; 7(1): 11-20.
doi: 10.1016/j.cmet.2007.10.002.

67. Ju YS, Alexandrov LB, Gerstung M, Martincorena I, Nik-Zainal S et al. Origins and functional consequences of somatic mitochondrial DNA mutations in human cancer. eLife. 2014; 3, e02935.
doi:10.7554/eLife.02935

68. Xu XD, Shao SX, Jiang HP, Cao YW, Wang YH et al. Warburg effect or reverse Warburg effect? A review of cancer metabolism. Oncol Res Treat. 2015; 38, 117-122.
doi:10.1159/000375435

69. Weinhouse S.Hepatomas. Science. 1967: 158: 542-545.
doi:10.1126/science.158.3800.542

70. Zu XL, Guppy M. Cancer metabolism: facts, fantasy, and fiction. Biochem Biophys Res Commun. 2004; 313: 459-465.
doi: 10.1016/j.bbrc.2003.11.136.

bioRxiv preprint doi: https://doi.org/10.1101/674150; this version posted June 18, 2019. The copyright holder for this preprint (which was not certified by peer review) is the author/funder, who has granted bioRxiv a license to display the preprint in perpetuity. It is made available under aCC-BY 4.0 International license.

71. Potter M, Newport E, Morten KJ. The Warburg effect: 80 years on. Biochem Soc Trans. 2016; 44(5): 1499-1505.
doi: 10.1042/BST20160094.

72. Yu H, Bian X, Gu D, He X. Metformin synergistically enhances cisplatin-induced cytotoxicity in esophageal squamous cancer cells under glucose-deprivation conditions. Biomed Res. 2016; 8678634.
doi: 10.1155/2016/8678634.

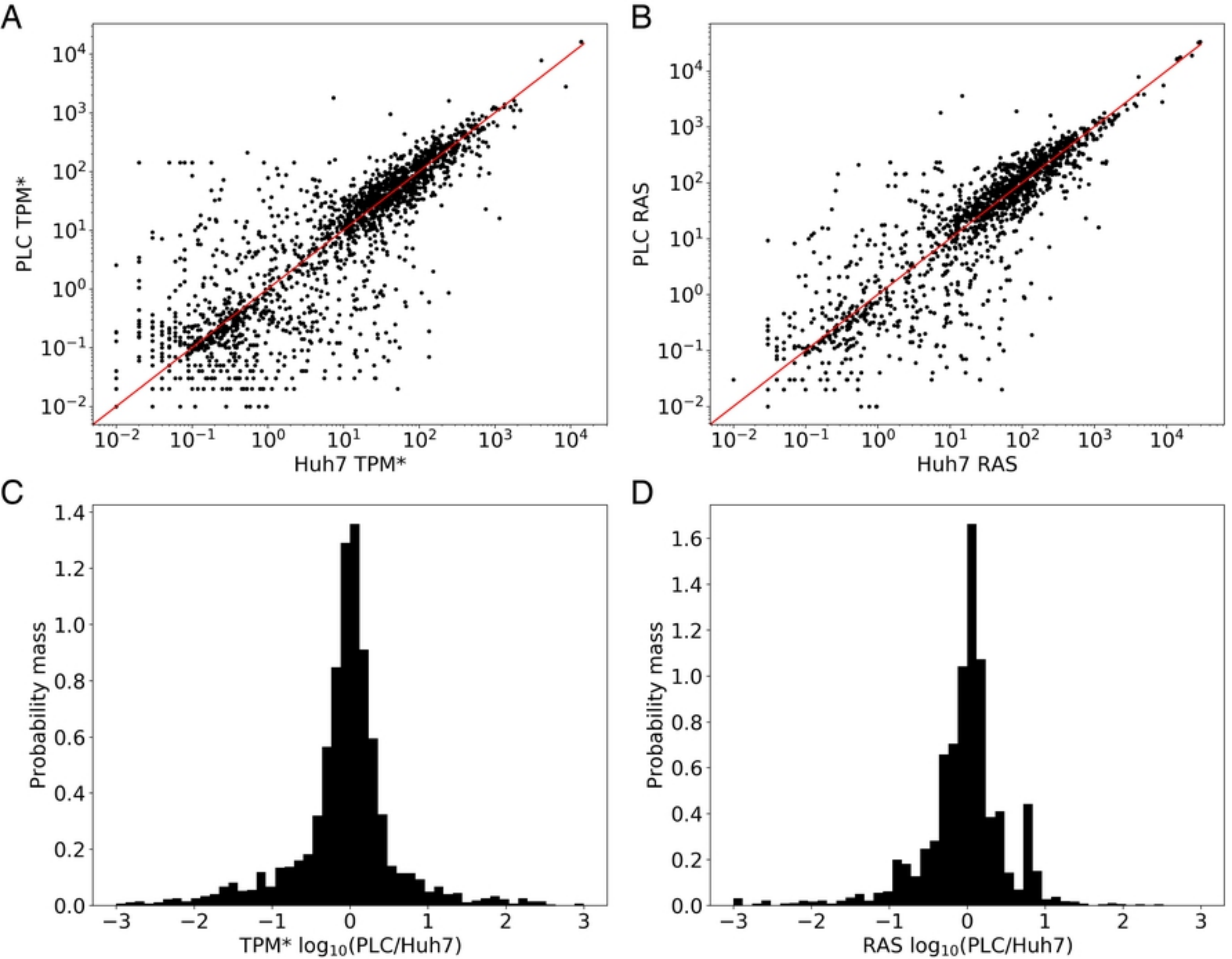
A
PLC TPM*
Huh7 TPM*
B
PLC RAS
Huh7 RAS
C
Probability mass
TPM* log10(PLC/Huh7)
D
Probability mass
RAS log10(PLC/Huh7)

Figure_1

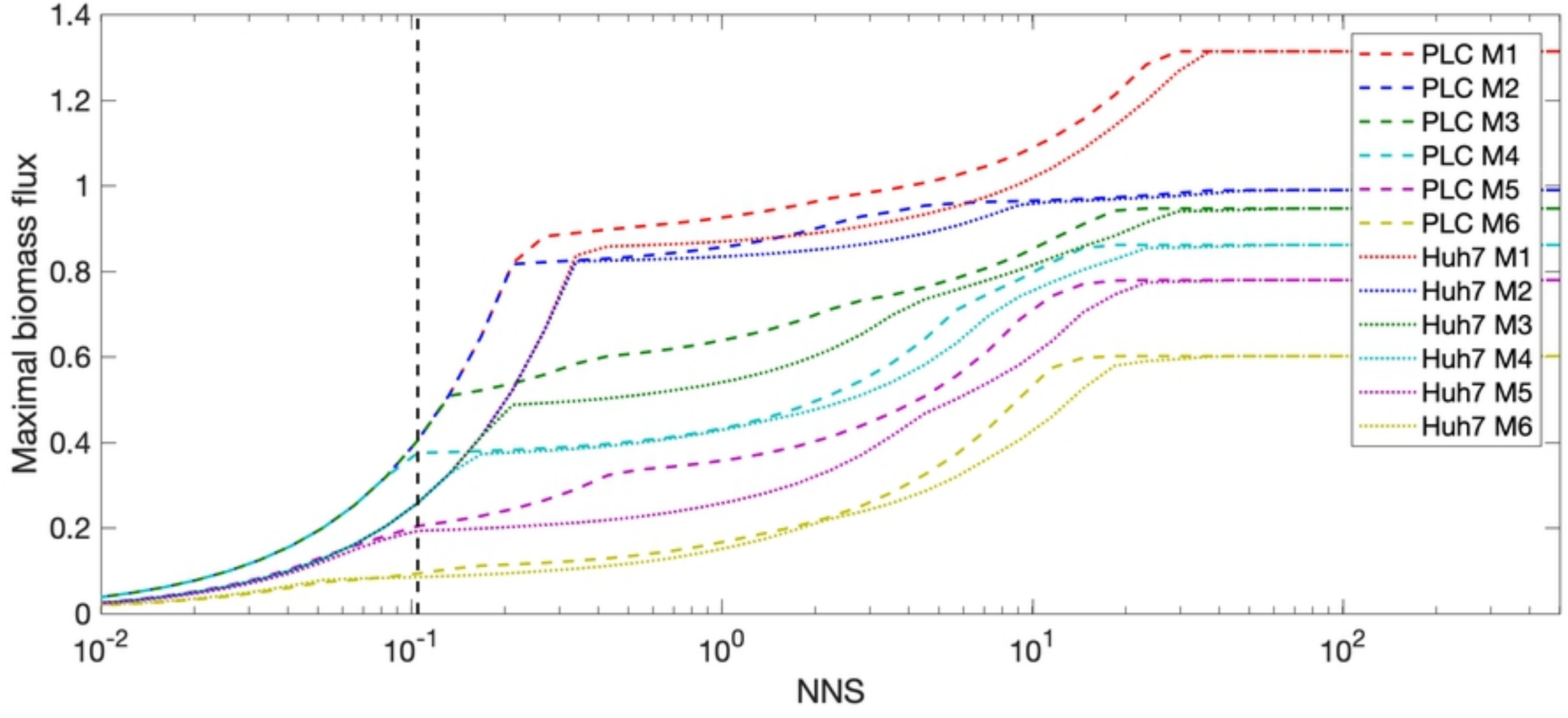
Maximal biomass flux
NNS
1.4
1.2
1
0.8
0.6
0.4
0.2
0
10^{-2}
10^{-1}
10^{0}
10^{1}
10^{2}
PLC M1
PLC M2
PLC M3
PLC M4
PLC M5
PLC M6
Huh7 M1
Huh7 M2
Huh7 M3
Huh7 M4
Huh7 M5
Huh7 M6

Figure_2

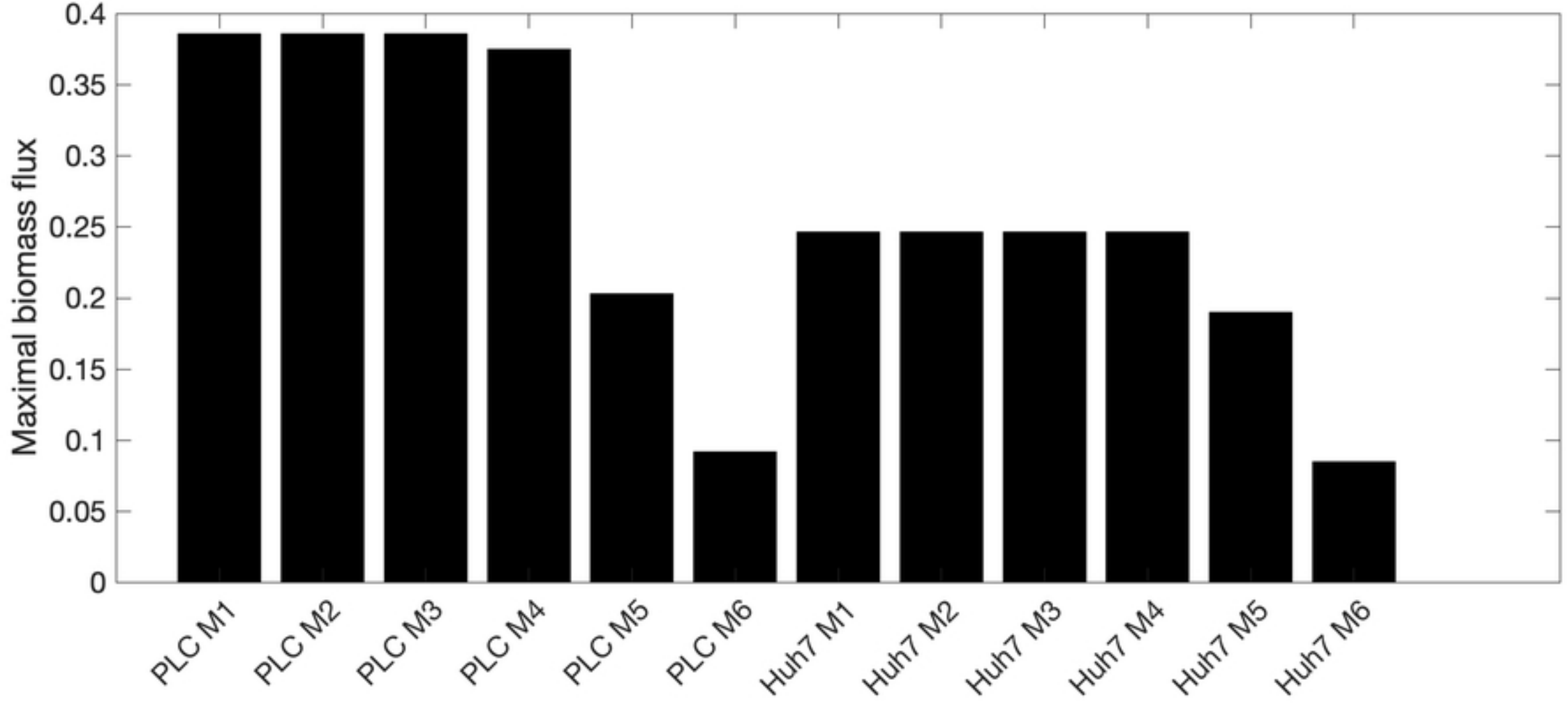
Maximal biomass flux
0.4
0.35
0.3
0.25
0.2
0.15
0.1
0.05
0
PLC M1
PLC M2
PLC M3
PLC M4
PLC M5
PLC M6
Huh7 M1
Huh7 M2
Huh7 M3
Huh7 M4
Huh7 M5
Huh7 M6

Figure_3

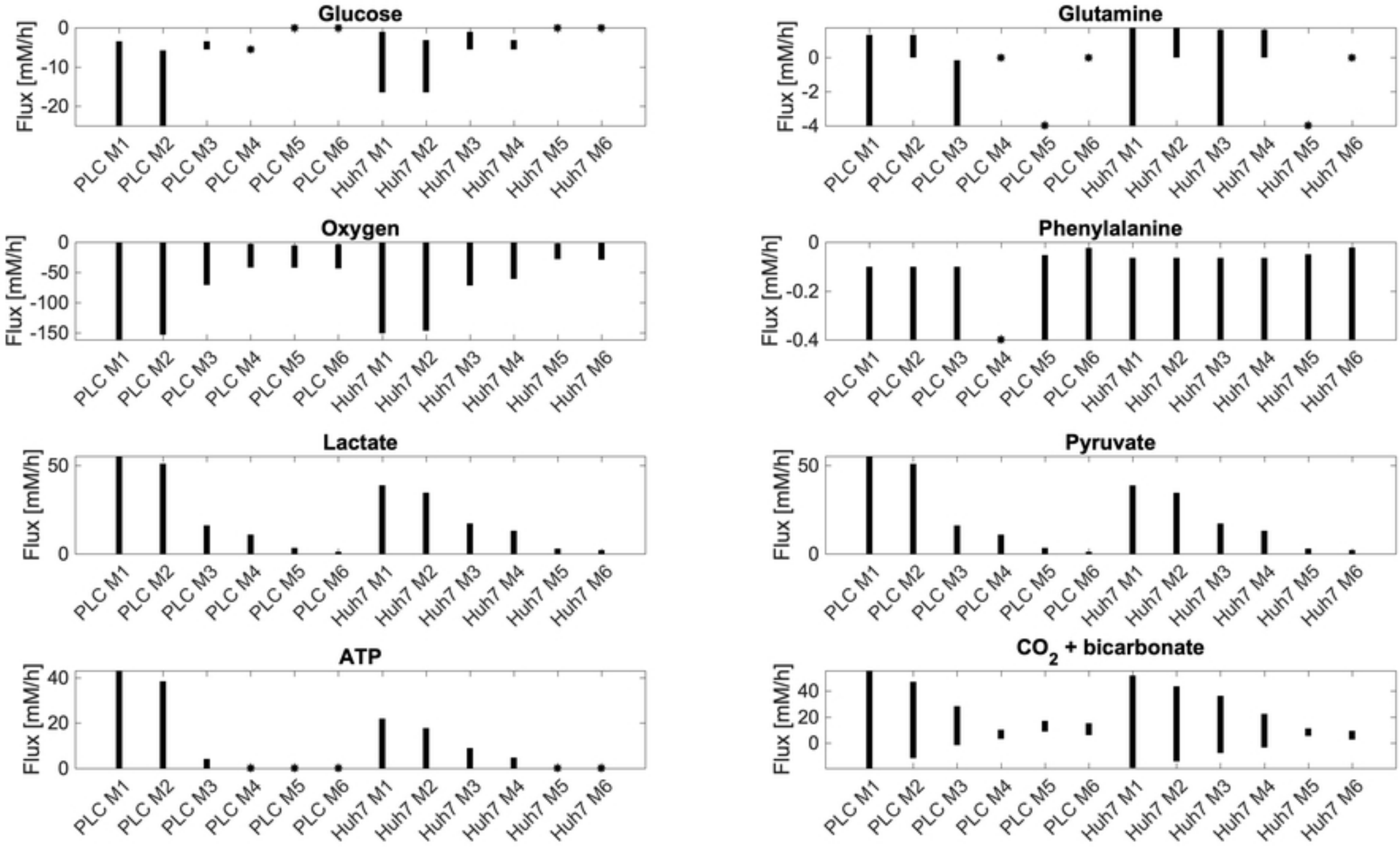
Glucose
Glutamine
Oxygen
Phenylalanine
Lactate
Pyruvate
ATP
CO_2 + bicarbonate
Flux [mM/h]
PLC M1
PLC M2
PLC M3
PLC M4
PLC M5
PLC M6
Huh7 M1
Huh7 M2
Huh7 M3
Huh7 M4
Huh7 M5
Huh7 M6

Figure_4

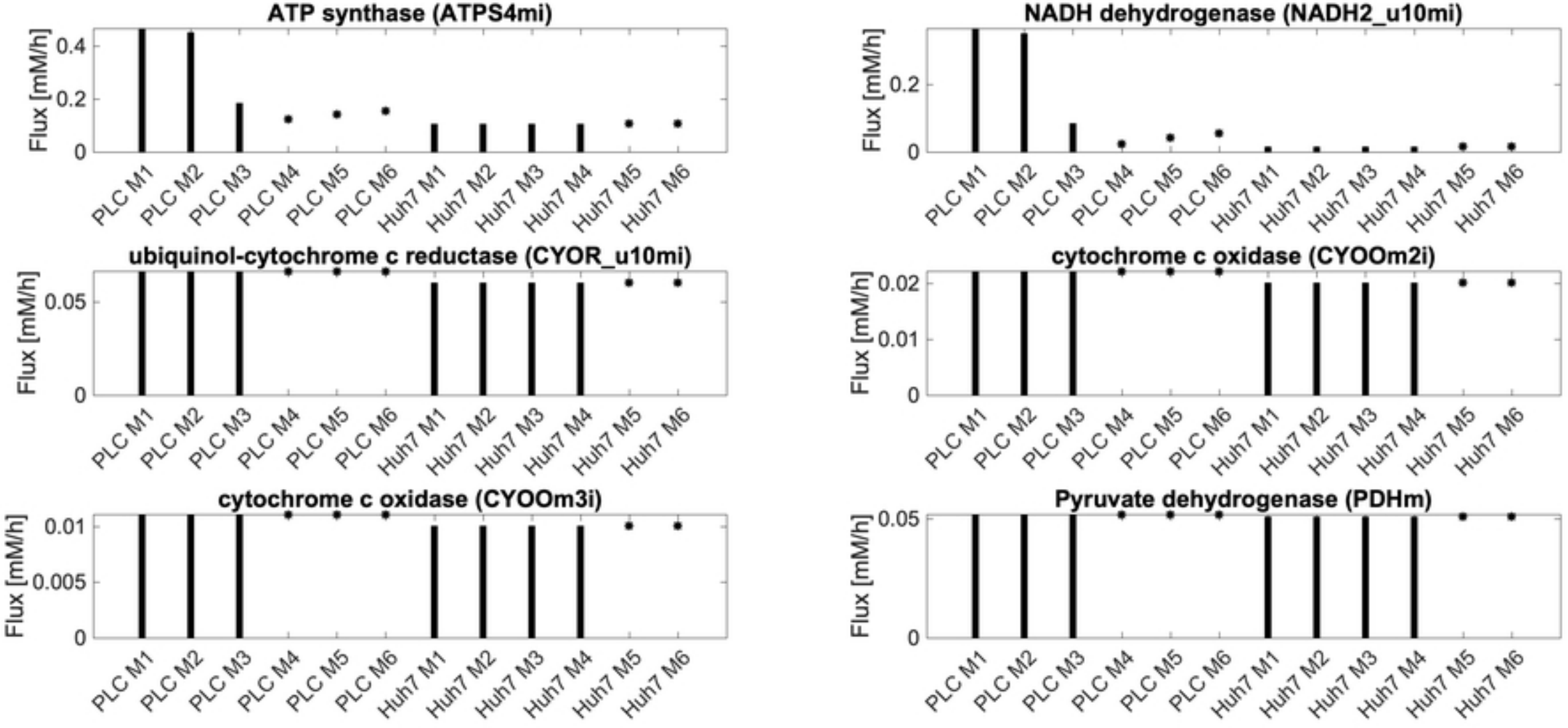
ATP synthase (ATPS4mi)
NADH dehydrogenase (NADH2_u10mi)
ubiquinol-cytochrome c reductase (CYOR_u10mi)
cytochrome c oxidase (CYOOm2i)
cytochrome c oxidase (CYOOm3i)
Pyruvate dehydrogenase (PDHm)
Flux [mM/h]
PLC M1
PLC M2
PLC M3
PLC M4
PLC M5
PLC M6
Huh7 M1
Huh7 M2
Huh7 M3
Huh7 M4
Huh7 M5
Huh7 M6

Figure_5

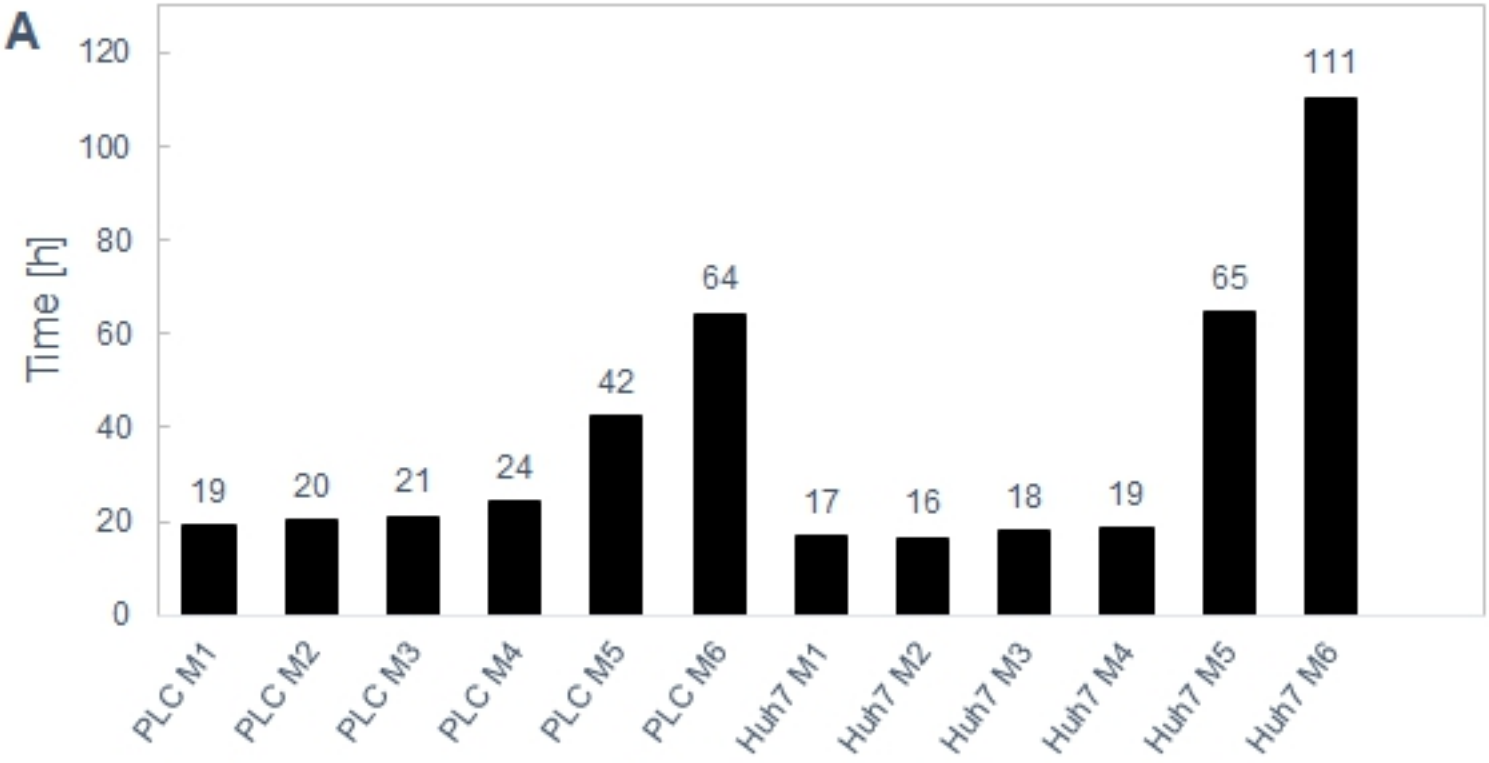
A
Time [h]
120
100
80
60
40
20
0
19
20
21
24
42
64
17
16
18
19
65
111
PLC M1
PLC M2
PLC M3
PLC M4
PLC M5
PLC M6
Huh7 M1
Huh7 M2
Huh7 M3
Huh7 M4
Huh7 M5
Huh7 M6

Figure_6

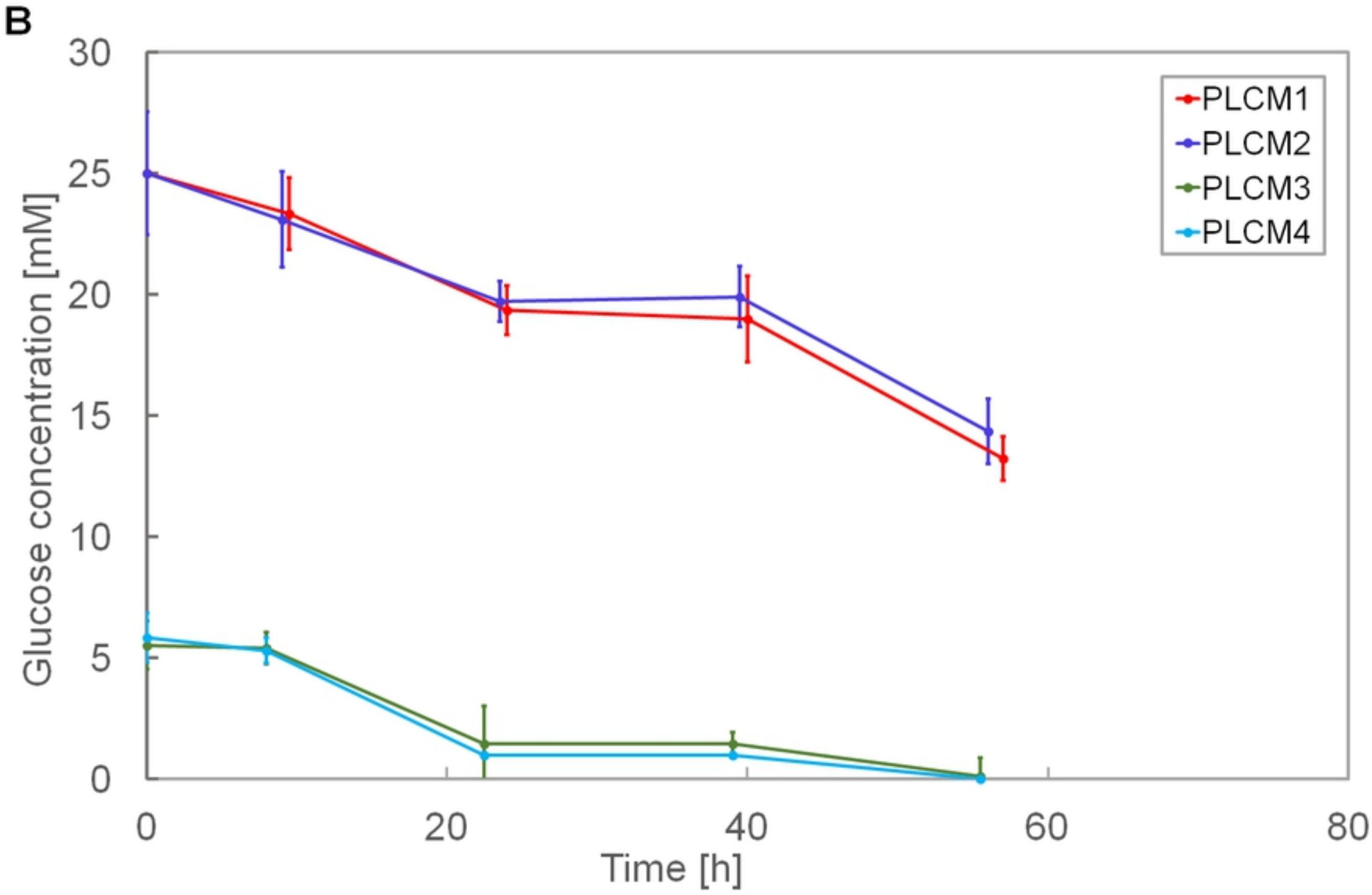
B
30
25
20
15
10
5
0
Glucose concentration [mM]
0
20
40
60
80
Time [h]
PLCM1
PLCM2
PLCM3
PLCM4

Figure_7

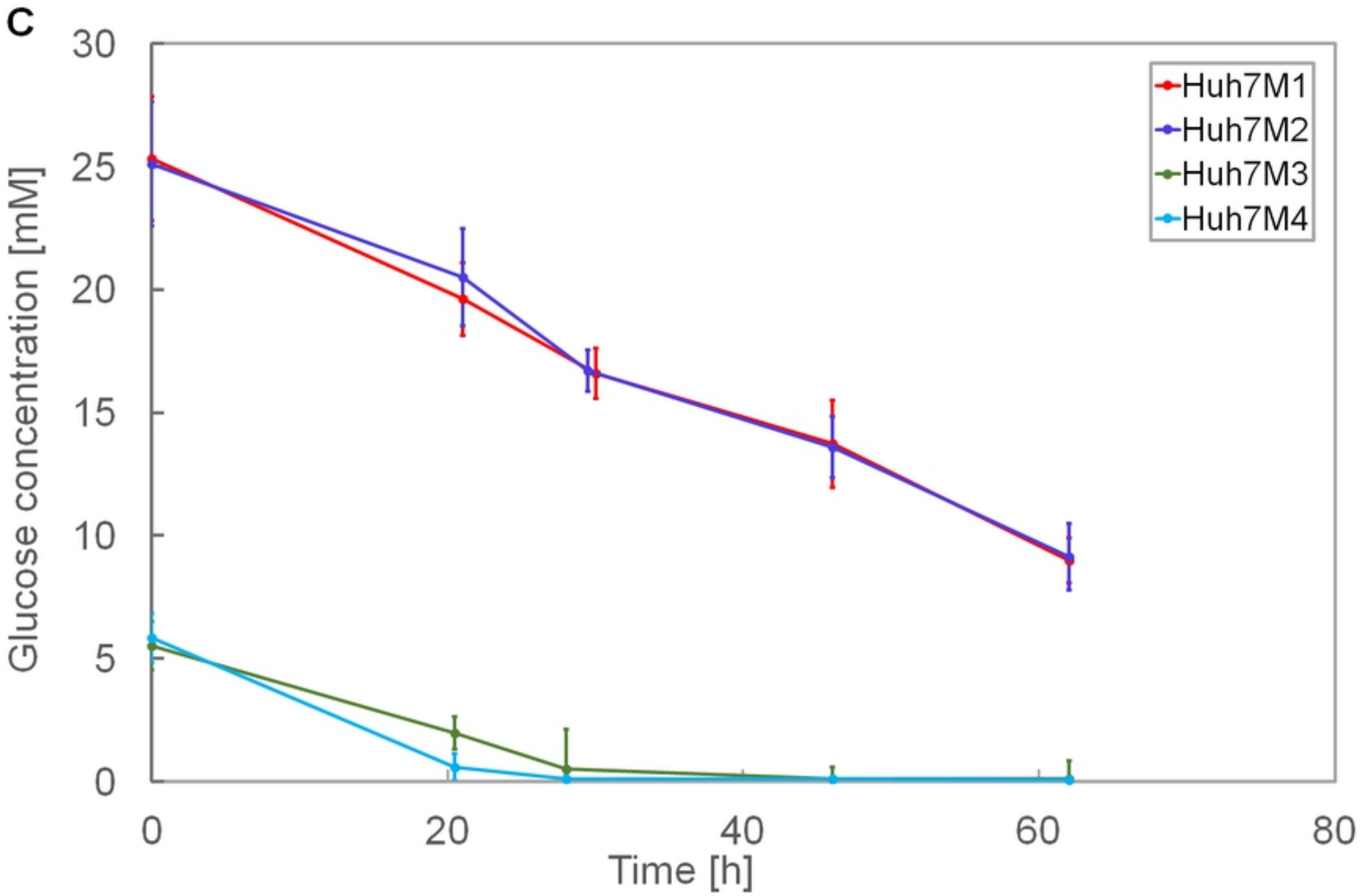
c
Huh7M1
Huh7M2
Huh7M3
Huh7M4
Glucose concentration [mM]
30
25
20
15
10
5
0
0
20
40
60
80
Time [h]

Figure_8

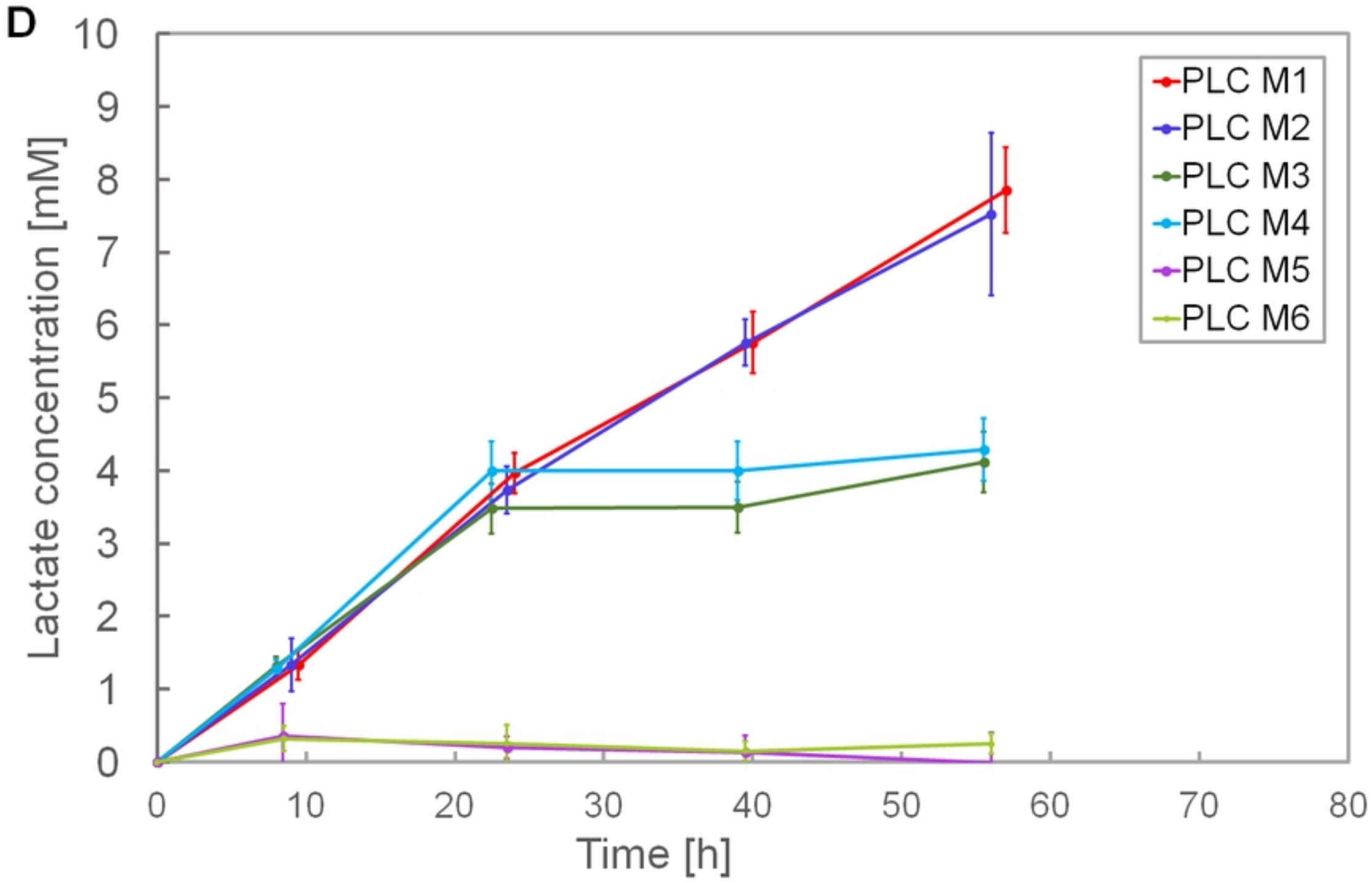
D
Lactate concentration [mM]
Time [h]
PLC M1
PLC M2
PLC M3
PLC M4
PLC M5
PLC M6
0
1
2
3
4
5
6
7
8
9
10
0
10
20
30
40
50
60
70
80

Figure_9

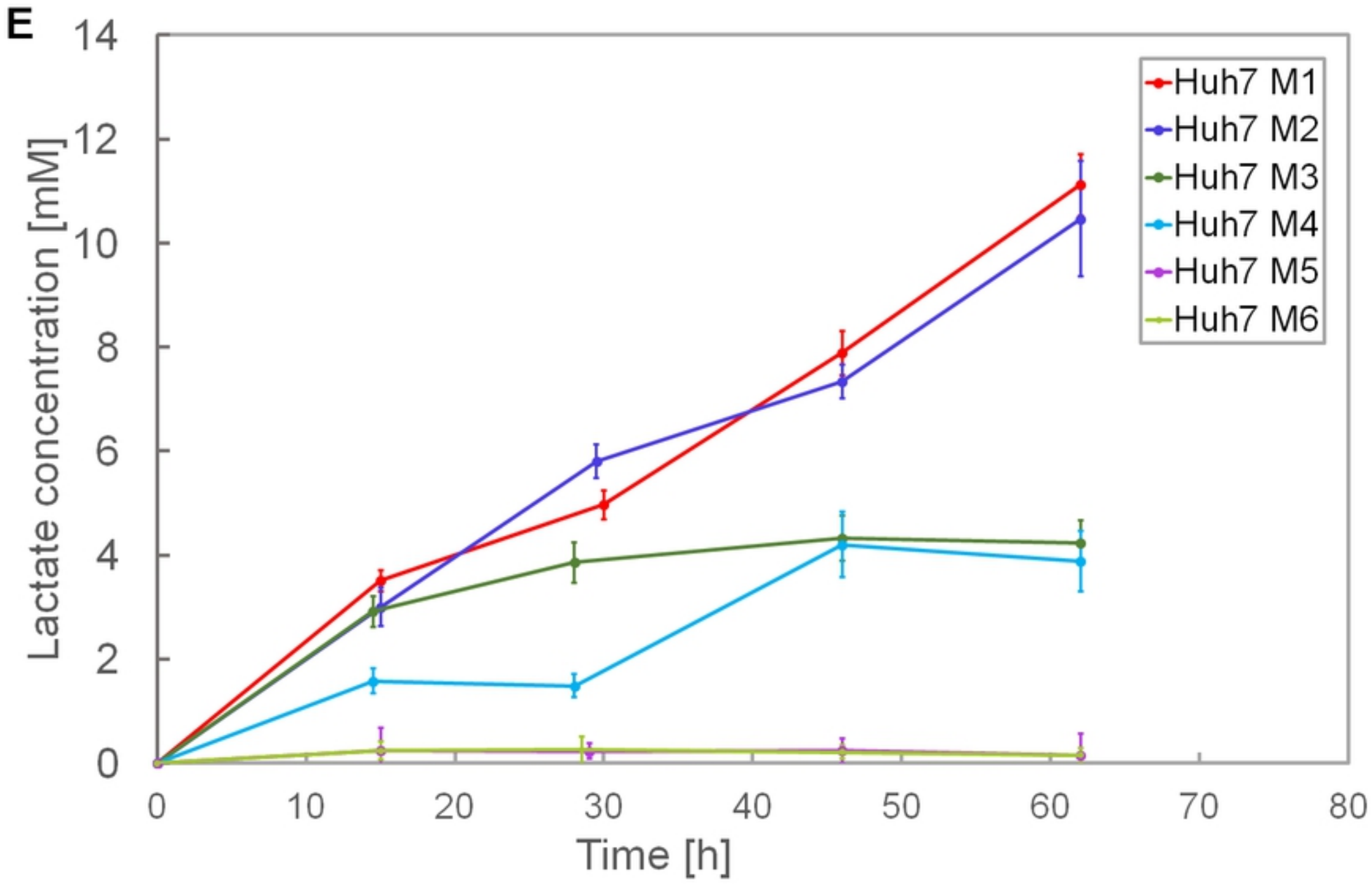
E
Lactate concentration [mM]
Time [h]
Huh7 M1
Huh7 M2
Huh7 M3
Huh7 M4
Huh7 M5
Huh7 M6
0
2
4
6
8
10
12
14
0
10
20
30
40
50
60
70
80

Figure_10

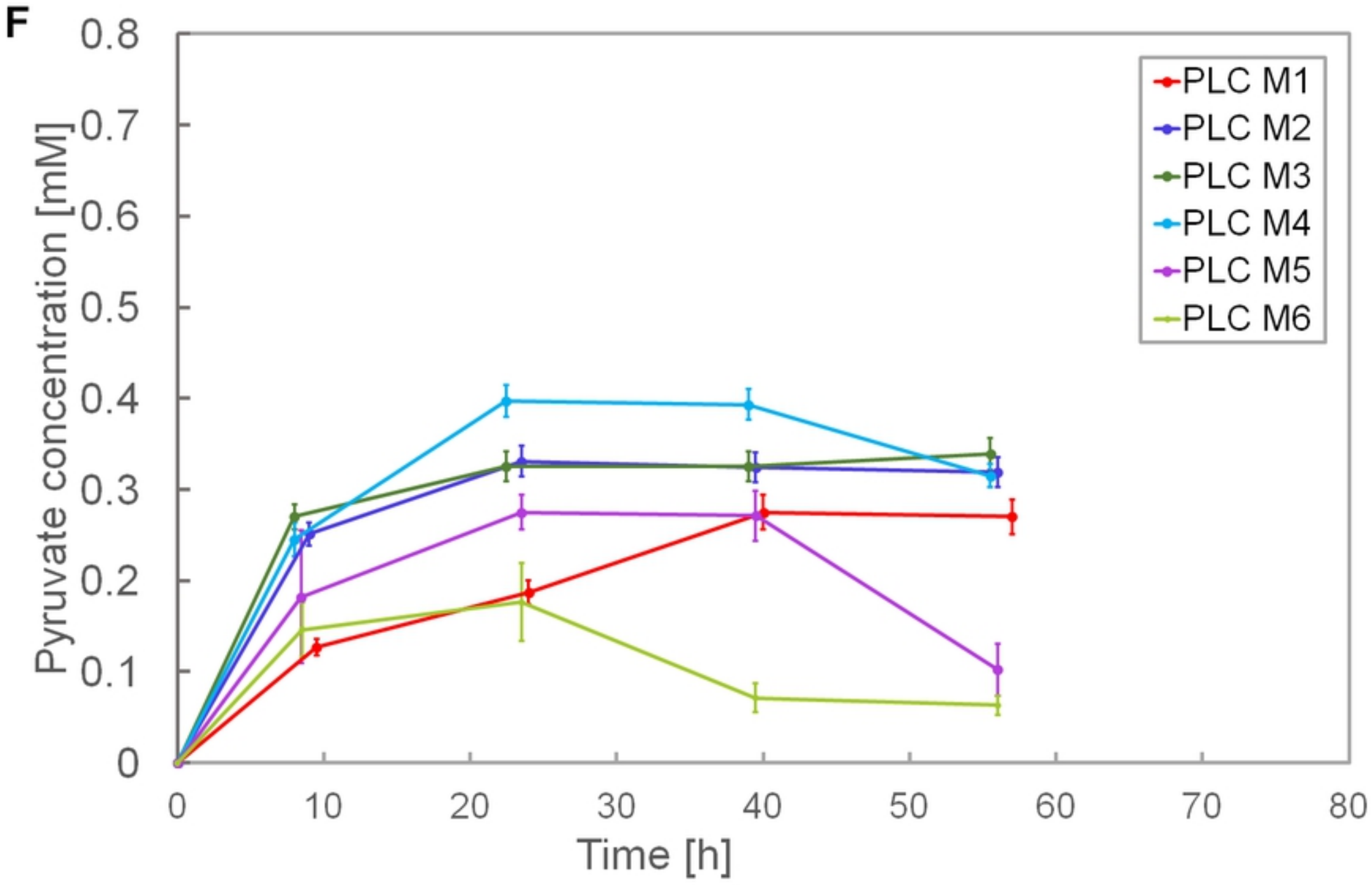
F
0.8
0.7
0.6
0.5
0.4
0.3
0.2
0.1
0
Pyruvate concentration [mM]
0
10
20
30
40
50
60
70
80
Time [h]
PLC M1
PLC M2
PLC M3
PLC M4
PLC M5
PLC M6

Figure_11

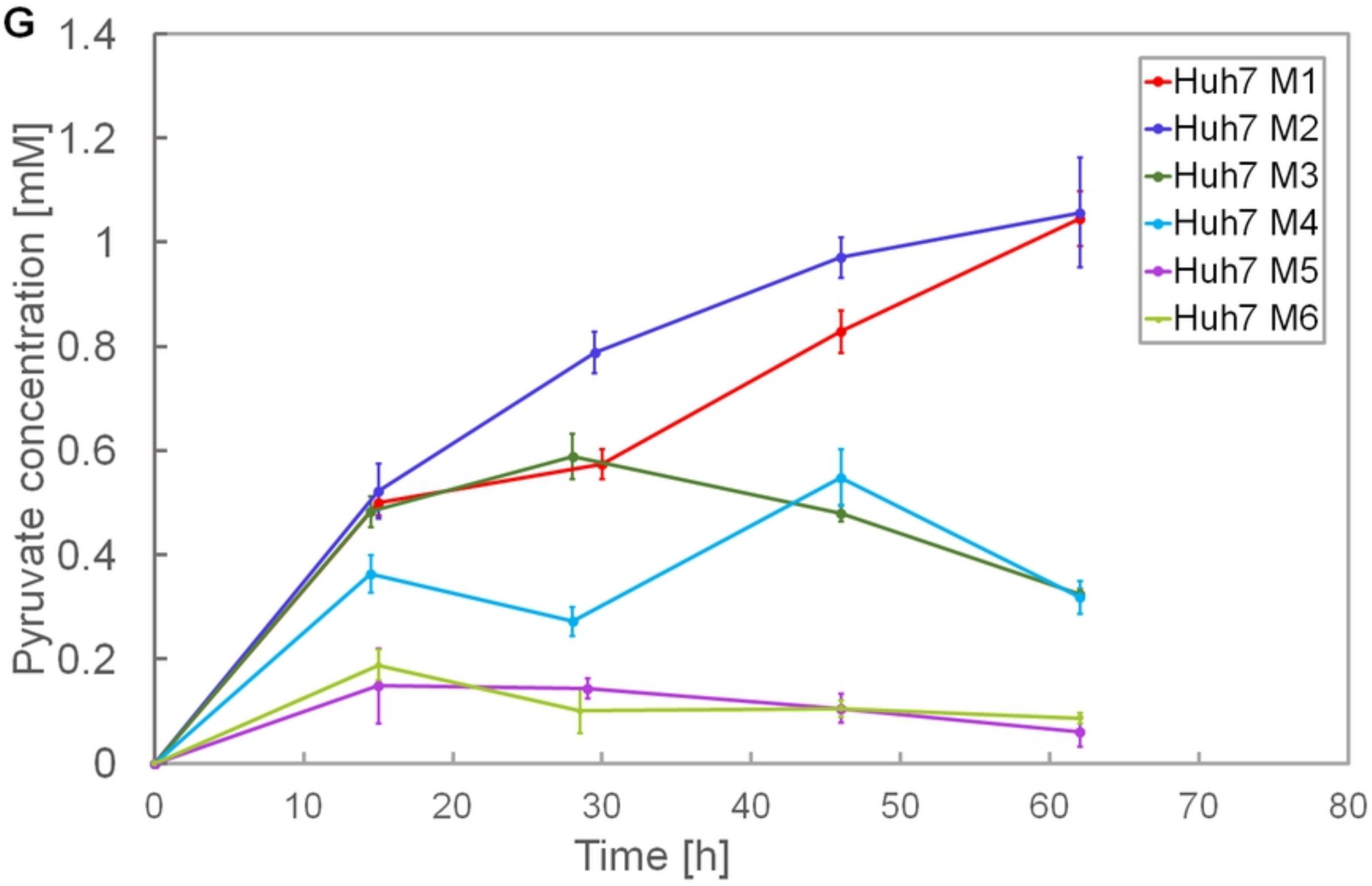
G
Pyruvate concentration [mM]
1.4
1.2
1
0.8
0.6
0.4
0.2
0
0
10
20
30
40
50
60
70
80
Time [h]
Huh7 M1
Huh7 M2
Huh7 M3
Huh7 M4
Huh7 M5
Huh7 M6

Figure_12

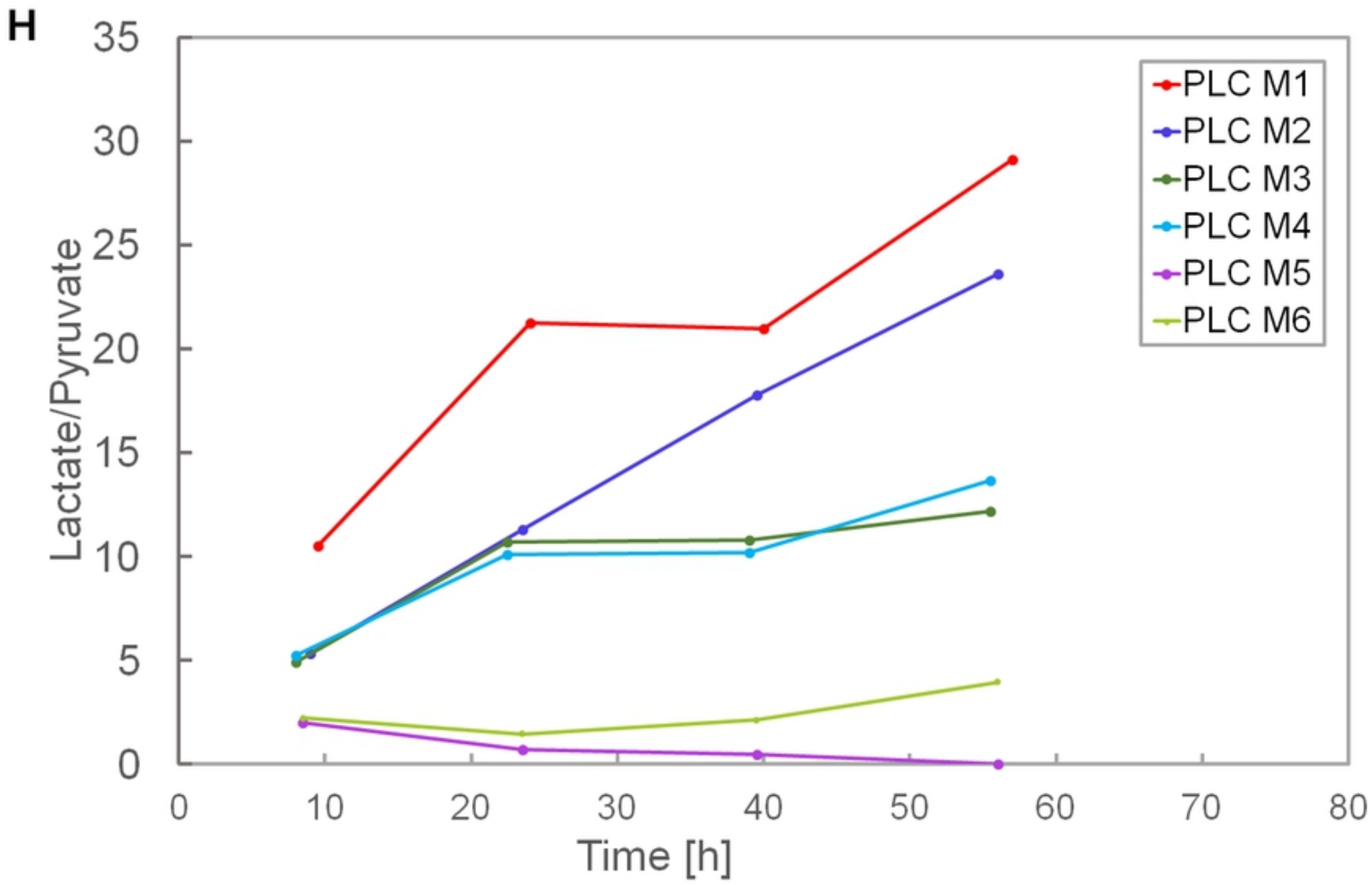
H
35
30
25
20
15
10
5
0
Lactate/Pyruvate
0
10
20
30
40
50
60
70
80
Time [h]
PLC M1
PLC M2
PLC M3
PLC M4
PLC M5
PLC M6

Figure_13

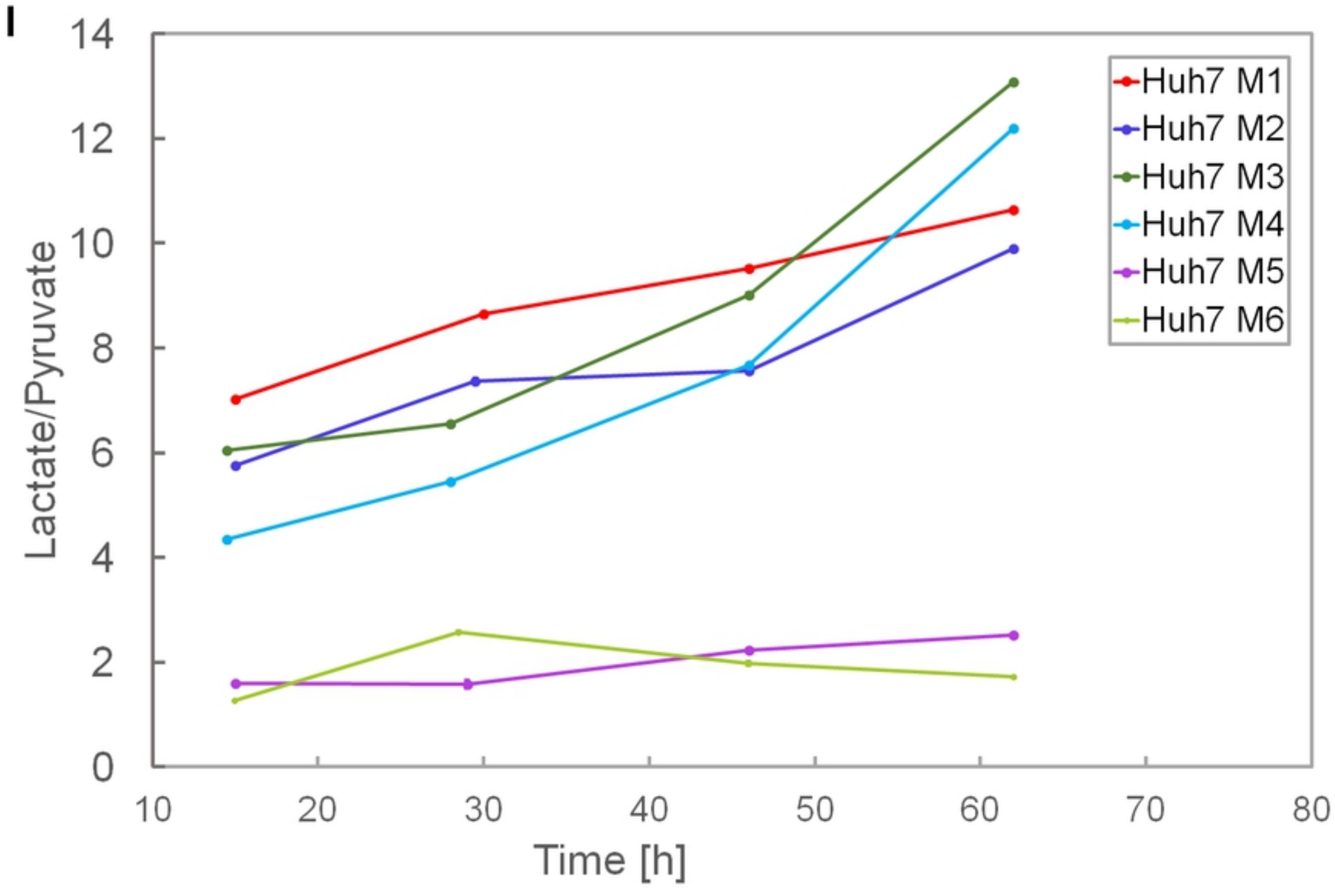
I
14
12
10
8
6
4
2
0
Lactate/Pyruvate
10
20
30
40
50
60
70
80
Time [h]
Huh7 M1
Huh7 M2
Huh7 M3
Huh7 M4
Huh7 M5
Huh7 M6

Figure_14

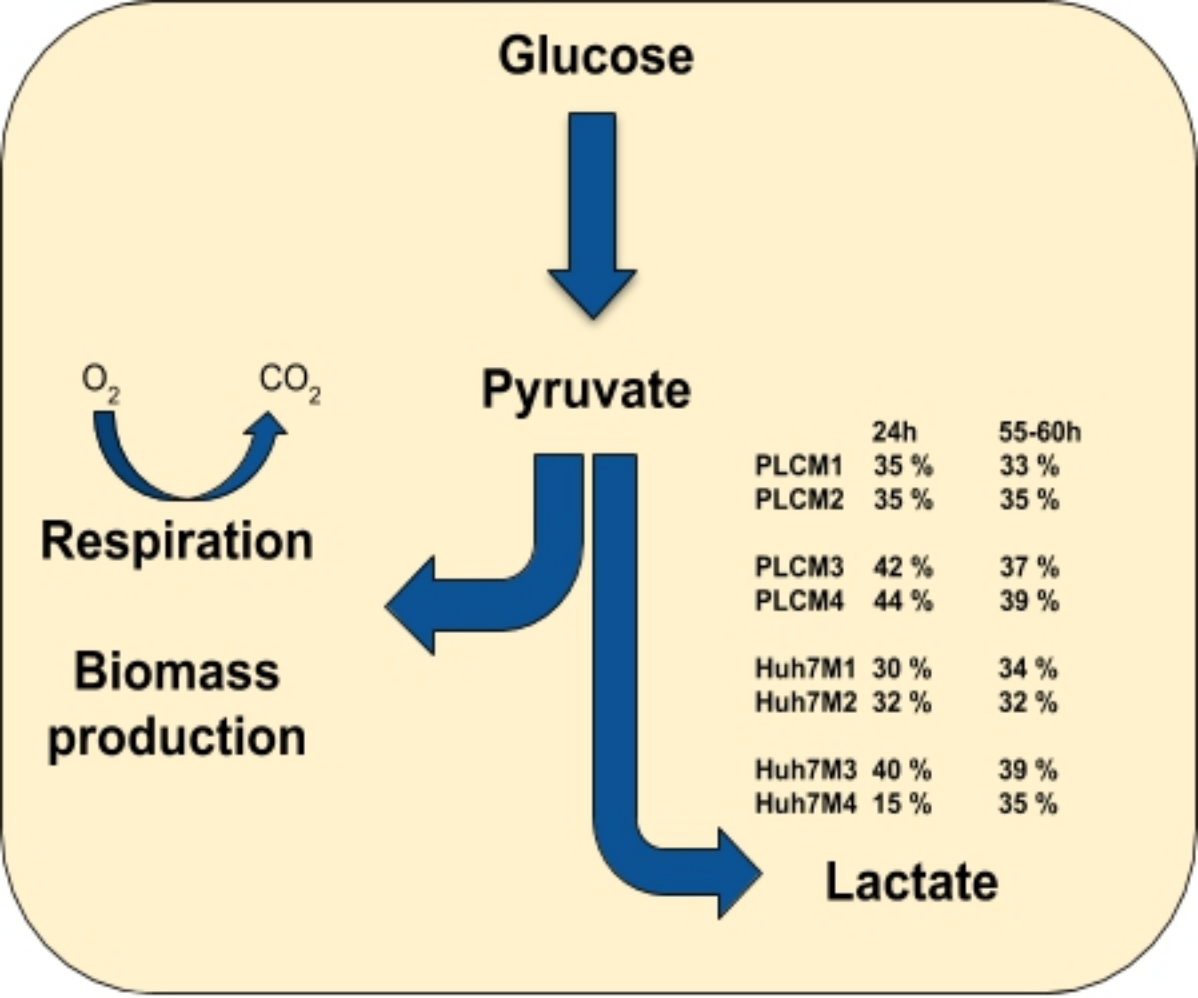
Glucose
Pyruvate
O_2
CO_2
Respiration
Biomass production
Lactate
24h 55-60h
PLCM1 35 % 33 %
PLCM2 35 % 35 %
PLCM3 42 % 37 %
PLCM4 44 % 39 %
Huh7M1 30 % 34 %
Huh7M2 32 % 32 %
Huh7M3 40 % 39 %
Huh7M4 15 % 35 %

Figure_15